

ICCESEN-2021

8th International Conference on Computational and Experimental Science and Engineering

Online-TURKEY

27-31 October 2021

Proceedings of ICCESEN-2021

EDITORS

Prof.Dr. İskender AKKURT

Dr. Kadir GÜNOĞLU

Dr. Hakan AKYILDIRIM

ISBN : 978-605-68728-0-8

iccesen2021@gmail.com

2021.iccesen.org

ICCESEN-2021

8th International Conference on Computational and Experimental Science and Engineering
Online-TURKEY
27-31 October 2021

Proceedings of ICCESEN-2021

Editors:

Prof.Dr. İskender AKKURT

Dr. Kadir GÜNOĞLU

Dr. Hakan AKYILDIRIM

ISBN: 978-605-68728-0-8

Proceedings of ICCESEN-2021 ,

8th International Conference on Computational and Eperimental Science and Engineering (**ICCESEN-2021**)

27-31 October 2021, Online-TURKEY

Editors:

Prof. Dr. İskender AKKURT

Dr. Kadir GÜNOĞLU

Dr. Hakan AKYILDIRIM

Published : 30 December 2021

ISBN: 978-605-68728-0-8

This work is subject to copyright. All rights are reserved, whether the whole or part of the material is concerned. Nothing from this publication may be translated, reproduced, stored in a computerized system or published in any form or in any manner, including, but not limited to electronic, mechanical, reprographic or photographic, without prior written permission from the Publisher 2020.iccesen.org . Pls contact at iccesen2020@gmail.com.

The individual contributions in this publication and any liabilities arising from them remain the responsibility of the authors. The publisher is not responsible for possible damages, which could be a result of content derived from this publication.

TABLE OF CONTENTS

TABLE OF CONTENTS	i
FOREWORD	v
ORGANISATION COMMITTEE	vi
SCIENTIFIC COMMITTEE	vii
INVITED SPEAKERS	ix
Wenli KE, Yuetian LIU, Songqi LI, Gaoming YU “Review on the Threshold Pressure Gradient in Heavy Oil Reservoirs”	1-6
İlyas KARTAL, Kadir GÜNOĞLU, İskender AKKURT “The impact of Al ₂ O ₃ doping in vinyl ester resin on gamma radiation attenuation coefficient”	7-9
Songqi LI, Yuetian LIU, Wenli KE, Jun LI , “Experimental Study on the Effect of Key Ions in Smart Water Flooding for Carbonate Reservoirs in Middle East”	10-13
Mohammed A.M. ALNASER, Kadir GÜNOĞLU, Nermin DEMİRKOL, İskender AKKURT , “Behavior of some ceramic materials against gamma ray with 662 keV energy”	14-16
Songqi LI, Yuetian LIU, Wenli KE, Jun LI , “Experimental Study on Chemistry of Produced Oil in Carbonate Reservoirs During High- and Low-Salinity Water Flooding”	17-19
İmad H.SHARQI, Kadir GÜNOĞLU, Hakan AKYILDIRIM, İskender AKKURT, Taner KAVAS , “Investigation of gamma-ray shielding properties of waste medical glass at 511 keV”	20-22
Şemsettin KILINÇARSLAN, Yasemin ŞİMŞEK TÜRKER , “Reinforcement of Glulam Beams with Carbon-FRP”	23-26
Simge ÇABUK, Erman DUMAN, Kadir GÜNOĞLU, İskender AKKURT , “The 40K natural radionuclide concentration in some medicinal aromatic plants”	27-29
Şemsettin KILINÇARSLAN, İskender AKKURT, Yasemin ŞİMŞEK TÜRKER, Kadir GÜNOĞLU , “Investigation of Radiation Shielding Properties of Wood Material”	30-33
Aycan SAHİN, Kadir GÜNOĞLU, Hakan AKYILDIRIM, İskender AKKURT , “Experimental investigation of biomaterials for gamma ray protection”	34-37

FOREWORD



Dear Colleagues,

It is a great honor for me to host you all in “**8th International Conference on Computational and Experimental Science and Engineering (ICCESSEN-2021)**” was taken as Online-TURKEY due to the Covid-19 in the period of 27-31 October 2021.

We are also happy to publish the proceeding of ICCESSEN-2021. All papers have been reviewed by two reviewers.

Prof. Dr. İskender AKKURT

Chair for ICCESSEN-2021

Editor for Proceedings of ICCESSEN-2021

ORGANISATION COMMITTEE

Prof.Dr. Iskender AKKURT (Chair)	Suleyman Demirel University, Isparta -Turkey
Dr. Kadir GÜNOĞLU (secretary)	Isparta Uygulamalı Bilimler University, Isparta -Turkey
Dr. Hakan AKYILDIRIM	Suleyman Demirel University, Isparta -Turkey
Dr. Ahmet BEYÇİOĞLU	Düzce University, Düzce -Turkey
Dr. Nilgün DEMİR	Uludag University, Bursa -Turkey
Dr. Nurdan KARPUZ DEMİR	Suleyman Demirel University, Isparta -Turkey
Dr. Özge Kozguş GÜLDÜ	Ege University,İzmir-Turkey
Dr. Ümit KARA	Suleyman Demirel University, Isparta -Turkey
Dr. Feride KULALI	Üsküdar University, Istanbul-Turkey
Dr. Zehra Nur KULUÖZTÜRK	Bitliseren University, Bitlis-Turkey
Dr. M. Fatih KULUÖZTÜRK	Bitliseren University, Bitlis-Turkey
Dr. Hüseyin Ozan TEKİN	Üsküdar University, Istanbul-Turkey

SCIENTIFIC COMMITTEE

Prof.Dr. Iskender AKKURT (Chair)	Suleyman Demirel University, Isparta –Turkey
Prof.Dr. Majid ABBASPOUR	Sharif University of Technology-Iran
Prof.Dr. Zahid Hussain ABRA	Quadi-E-Awam University, Sindh-Pakistan
Prof.Dr. Abdullah ALAMRI	King Saud University, Saudi Arabia
Prof.Dr. Nezam Mahdavi-AMIRI	Sharif University Iran
Dr. John R.M.ANNAND	Glasgow University, Glasgow-Scotland (UK)
Dr. Majda AOUITITEN	Abdelmalek Essaadi University-Morocco
Prof.Dr. Mohamed Kheireddine AROUA	University of Malaya-Malaysia
Dr. Rachid BELKADA	CRSTSE -Algeria
Dr. Radhey S BENIWAL	CSIR-NISCAIR, New Delhi 110012, India
Dr. Mahmoud Abdullah BENNASER	Kuwait University-Kuwait
Dr. Djoudi BOUHAFS	Centre de Recherche en Technologie -Algeria
Prof. Oleg BURDAKOV	Linköping University Linköping, Sweden
Dr. Yusuf CEYLAN	Selcuk University, Konya-Turkey
Prof.Dr. Lotfi CHOUGHANE	Weill Cornell Medical College-Qatar
Dr. Manju D CHOUDHARY	Niscair-India
Dr. Nermin DEMİRKOL	Kocaeli University, Kocaeli –Turkey
Prof.Dr. İbrahim DİNÇER	University of Ontario Institute of Technology (UOIT)-Canada
Prof. Dr. Mitra DJAMAL	Institute Teknologi Bandung-Indonesia
Prof.Dr. Mahmut DOĞRU	Bitlis Eren University, Bitlis-Turkey
Prof.Dr. Mohammed Mostafa EL TOKHI	United Arab Emirates University-UAE
Dr. Zuhair ER	Istanbul Technical University, Istanbul-Turkey
Prof.Dr. Mustafa EROL	Dokuz Eylul University, İzmir-Turkey
Prof.Dr. Madjid FATHI	Dept. of EECS University of Siegen- Germany
Prof.Dr. Jan FELBA	Wroclaw University of Technology-Poland
Prof.Dr. S. Mostafa GHIAASIAAN	Mechanical/Nuclear Engineering, Georgia Tech USA
Prof.Dr. Mustafa GÜNAL	Gaziantep University, Gaziantep-Turkey
Prof. Dr. Amir HUSSAIN	University of Stirling- Scotland(UK)
Dr. Nabi IBADOV	Warsaw University of Technology-Poland
Prof.Dr. Fatma KARİPCİN	Nevşehir Hacı Bektaş Veli University-Turkey
Prof.Dr. Hamdi Ş. KILIÇ	Selcuk University, Konya-Turkey
Dr. Menekşe V. KILIÇARSLAN	İstanbul Aydın University, Istanbul-Turkey

Prof.Dr. Ziya Erdem KOÇ	Selcuk University, Konya-Turkey
Prof. Dr. İsmail KOYUNCU	Istanbul Technical University, Istanbul-Turkey
Dr. Irida MARKJA	Polytechnic University, Tirana-Albania
Dr. F. Zümrüt Biber MÜFTÜLER	Ege University, Izmir-Turkey
Dr. Susan Shukur NOORI	Kirkuk University, Kirkuk-Iraq
Prof.Dr. Ravindra NUGGEHALLI	New Jersey Institute of Technology-USA
Prof.Dr. İbrahim ÖRÜN	Aksaray University, Aksaray-Turkey
Prof.Dr. Necati ÖZDEMİR	Balıkesir University, Balıkesir-Turkey
Dr. Zeynep PARLAR	Istanbul Technical University, Istanbul-Turkey
Prof.Dr. Ioana G. Petrisor	ToxStrategies, Inc., Mission Viejo, CA
Dr. Tomasz PIOTROWSKI	Warsaw University of Technology, Warsaw-Poland
Prof.Dr. Javad RAHIGHI	AEOI, Tehran-Iran.
Dr. Abdelmadjid RECIQUI	University of Boumerdes-Algeria
Prof.Dr. Osman SAGDIÇ	Yıldız Technical University, Istanbul-Turkey
Prof.Dr. Miljko SATARIC	Faculty of Technical Sciences Novi Sad-Serbia
Prof.Dr. Saleh SULTANSOY	TOBB University, Ankara-Turkey
Dr. Naim SYLA	University of Prishtina-Kosova
Prof. Dr. Mustafa TAVASLI	Uludag University, Bursa-Turkey
Dr. Huseyin TOROS	Istanbul Technical University, Istanbul-Turkey
Prof.Dr. Ahmad UMAR	Najran University-Saudi Arabia
Prof.Dr. Gerhard-Wilhelm WEBER	Middle East Technical University Ankara-Turkey
Prof.Dr. Erol YAŞAR	Mersin University, Mersin-Turkey

INVITED SPEAKERS

	<p>Prof. Dr. Amir HUSAIN <i>Napier University, Edinburg, Scotland-UK</i></p> <p>Title: Big Data Application in Science</p>
	<p>Dr. Gökçe ŞIRVANLI <i>Ufuk University, Ankara, TURKEY</i></p> <p>Title: Stress and Music from a Neuroscience Perspective: A Model of Wellbeing</p>
	<p>Prof. Dr. Madjid FATHI <i>Dept. of EECS University of Siegen, GERMANY</i></p> <p>Title: AI and Knowledge graphs for integrating cyber physical resources</p>
	<p>Dr. Samira FETNI <i>University of Batna2-ALGERIA</i></p> <p>Title: Genetic variants and mutations of SARS-CoV-2, vaccines and non specific immunity</p>
	<p>Dr. Soumi DUTTA <i>Institute of Engineering & Management (IEM)-INDIA</i></p> <p>Title: Challenges in Social Network Data Analytics</p>



Prof.Dr. Gerhard-Wilhelm WEBER

Poznan University of Technology-POLAND

Title: Sustainable Aggregate Production Planning with Overtime,
Outsourcing and Human Factors under Uncertain Seasonal Demand

Review on the Threshold Pressure Gradient in Heavy Oil Reservoirs

Wenli KE1, Yuetian LIU1*, Songqi LI1, Gaoming YU2

1China University of Petroleum (Beijing) ,College of Petroleum Engineering, Beijing, CHINA

2 Yangtze University, College of Petroleum Engineering, Wuhan, China

*Yuetian Liu @institution.org

ABSTRACT

Flow of heavy oils in porous reservoirs does not follow the Darcy law. The heavy oil requires a certain threshold pressure gradient prior to flow initiation. The presence of the threshold pressure gradient changes sharply the flow pattern giving rise to stagnant zones in homogeneous fluid flow and to dead areas of motionless oil during water flooding. In recent years, many people focus on the mechanism, determination method, development and application in oilfield of threshold pressure gradient of heavy oil. The mechanism of threshold pressure gradient is mainly due to the molecular structure properties of heavy oil fluid, which is reflected in the rheology and intermolecular force of heavy oil. The method to determine the threshold pressure gradient mainly includes experimental method, numerical calculation and come from well test interpretation data. The application of threshold pressure gradient includes seepage formula revision, well pattern and spacing determination, residual oil distribution and productivity prediction. Here, we provide an integrated overview of recent advances in the mechanism, determination method, development and application in oilfield of the threshold pressure gradient of heavy oil and corresponding implications in recent oilfield studies.

KEYWORDS - *Heavy oil, The threshold pressure gradient, The measurement method, The mechanism.*

1. INTRODUCTION

The rate and ultimate recovery of heavy oil from petroleum reservoirs are strongly affected by their flowing characteristics in porous rock [1-6]. Frequently, the non-Newtonian characteristics of heavy oil are caused by asphaltene and other heavy components [6-15]. Most heavy oils have the properties of a Bingham fluid, i.e. when the shear stress exceeds the yield stress, the fluid becomes a Newtonian fluid [16-17].

Heavy oil is a complex mixture of hydrocarbons that is rich in wax, colloids and asphaltene with a high density, high viscosity and poor fluidity. With the increase in heavy oil exploitation in the world, heavy oil recovery technology, gathering and transporting technology, and long-distance transporting technology are continuously being improved [4]. Data show that with the continuous improvements in petroleum exploration and the development of technology in recent years, among the newly discovered petroleum geological reserves, the reserves of heavy oil resources in the world have reached ten times the reserves of conventional crude oil, which holds the strategic position of replacing conventional energy sources. However, due to the high viscosity of heavy oil, high seepage resistance and strong interaction between the liquid–solid and liquid–liquid interfaces, the seepage law of heavy oil deviates from Darcy’s law to some extent. Only when the driving pressure gradient exceeds the initial pressure gradient does the heavy oil begin to flow. This starting pressure gradient will change the law of oil and water migration in porous media, affecting the productivity of oil wells, which has an important impact on oilfield development. For many years, people have consistently tried to explore the reasons for the existence of the priming pressure gradient and find a method to accurately measure the priming pressure gradient [11]. Many researchers have made considerable progress. However, the understanding of the start-up pressure gradient is still in the initial stage. Even now, the mechanism of the start-up pressure gradient is still unclear, and there is no accurate or stable measurement method for the start-up pressure gradient.

2. MECHANISM OF THE THRESHOLD PRESSURE IN A HEAVY OIL RESERVOIR

2.1 Mechanism of the threshold pressure of single-phase seepage

For heavy oil reservoirs, the threshold pressure gradient controls the seepage of heavy oil, and the threshold pressure gradient is more meaningful than the critical pressure gradient[12].

In a porous medium, a heavy oil reservoir is similar to a low permeability reservoir, which has a non-Darcy flow with a threshold pressure gradient. The threshold pressure gradient of a low permeability reservoir is mainly caused by low permeability, while a heavy oil reservoir is due to the high viscosity and viscous forces of crude oil.

The threshold pressure gradient is controlled by the interactions at the solid–liquid interface. The higher the viscosity of the crude oil, the stronger the polarity, the greater the viscous force, and the larger the contact area with the pores[13]. The threshold pressure gradient increases as the viscosity of the crude oil increases. Because the viscosity of the crude oil decreases as the temperature increases, the threshold pressure gradient decreases as the temperature increases under the conditions of the porous medium. The permeability reflects the ability of the fluid to pass through the reservoir. The greater the permeability, the smaller the capillary pressure, the smaller the flow resistance and the smaller the threshold pressure gradient. The ultimate shear stress value is restricted by the interactions at the solid–liquid interface, and the main component affecting the solid–liquid interface is the crude oil macromolecule, asphaltene, whose content determines the polarity and viscosity of the crude oil.

2.2 Mechanism of the threshold pressure in two-phase seepage

The oil–water two-phase threshold pressure gradient refers to the pressure gradient that needs to be overcome when oil and water begin to flow under any water saturation when the oil and water are the same. There is a concept of comprehensive viscosity for oil–water co-infiltration, where the permeability is certain, and the threshold pressure gradient is mainly related to the viscosity of the fluid. Then, the water saturation increases, which is equivalent to the formation fluid being diluted, and the threshold pressure gradient is decreased[14].

The oil–water two-phase threshold pressure gradient includes two parts: one due to the viscous drag generated by the action of the fluid and the surface of the pores (same as the single-phase seepage starting pressure gradient) and the other part is the capillary resistance generated by the interaction between the two fluids.

During the oil–water two-phase percolation process, the oil and water flow along the pore space occupied by each and respectively interact with the pore wall surface to generate the respective boundary layer fluids and threshold pressure gradients; however, the flow of one phase inevitably pushes the other phase. Thus, the two-phase threshold pressure gradients must be equal. As the water saturation increases, the water flow channel increases, and the oil phase flows into the larger pores (hydrophilic formation), thus lowering the threshold pressure gradient.

The capillary phenomenon in low-permeability formation is prominent. Some oils in the pores are cut into large oil columns or oil beads. There are three kinds of capillary forces in the pores. First, the capillary force generated by the spherical meniscus at the oil–water contact surface is the first type. The capillary force is the driving force for water flooding. This force acts when the oil flow is continuous at the beginning of water flooding. Second, when the oil column that is cut off is large, an additional resistance is generated due to the deformation of the meniscus, which is the second type of capillary force[15].

In the case of high oil saturation, the oil flow is cut into oil columns due to the first capillary force, and the second type of capillary force is the main reason why the two-phase threshold pressure gradient is higher than the single-phase threshold pressure gradient.

The additional resistance generated by the non-wet-phase liquid droplets through the throat is the third type of capillary force. The oil-impacted oil in the later stage of water flooding produces a Jamin effect, which increases the flow resistance. However, due to the irregularity of the pores, the

wet-phase water can flow along the pore wall liquid layer under a large pressure difference, and the flow of the water phase can drive other oils that are not at the throat.

Therefore, the third type of capillary force acts to cause the two-phase threshold pressure gradient to be higher than the single-phase threshold pressure gradient. The pressure gradient of the aqueous phase under residual oil is higher than that of single-phase water, which is the effect of the Jamin effect. In summary, the combined effects of the three types of capillary forces cause the two-phase threshold pressure gradient to be higher than the single phase.

3. METHOD TO DETERMINE THE THRESHOLD PRESSURE GRADIENT

Researchers are working on the pressure gradient research related to nonlinear seepage and are continuously improving previous experimental methods and data processing methods. However, after years of hard work, there are still some issues with determining the threshold pressure gradient, which requires researchers to continuously study and solve the associated problems. Currently, there are three methods for determining the threshold pressure gradient: indoor physical experimental simulations, numerical experiments and well test interpretations[17-23].

(1) Physical simulation experiments

Percolation curve fitting method: The percolation curve is measured by a steady state method, and then the curve is fitted to obtain a threshold pressure gradient. The steady state method includes the constant pressure and constant current methods. The constant pressure method measures the pressure at the inlet end of the core by setting the pressure at the inlet end of the core until the flow reaches a stable value. Then, a gradual increase in the pressure at the inlet end of the core allows measurement of the steady flow at different pressures and plotting of the seepage curve according to the flow rate and pressure difference in the steady state. The constant current law allows us to set the flow rate at the inlet end of the core by recording the flow at the inlet end of the core and plot the seepage curve. Then, the threshold pressure gradient of the core is obtained by using the intercept of the curve on the pressure difference coordinate axis.

Unsteady method: The unsteady method is an experimental method for measuring pressure during unsteady seepage. This method is mainly used to determine the threshold pressure gradient when studying nonlinear seepage laws. By establishing the unstable seepage equation and solving the numerical solution via the finite difference method, the unstable dimensionless pressure curve at the closed end of the core can be obtained. On a double logarithmic graph, the measured pressure gradient and the theoretical dimensionless pressure curve can be fitted to determine the threshold pressure gradient of the core.

Capillary balance method: The capillary balance method is used to measure the threshold pressure gradient by using the principle of a connected device (as shown in Figure 16). When measuring the threshold pressure gradient, the capillary is connected at the inlet and outlet of the core. The action of gravity causes the fluid at the inlet end to flow through the core to the outlet end. When the liquid level at both ends is fully balanced, the height difference will eventually be maintained, which is the minimum threshold pressure of the sample.

Unsteady-displacement-capillary method: 'Unsteady-displacement-capillary metrology' involves filling the liquid at the outlet end of the core holder and then injecting the liquid at a micro-flow rate until the liquid level at the outlet end of the core begins to move. The pressure is the minimum threshold pressure. Li Ai Fen established a new 'capillary balance method', which involves driving a small flow rate to the core end of the core to begin the flow, closing the inlet switch, recording the height of the liquid column on a mercury differential pressure meter at different times until the liquid column becomes highly stable, resulting in calculating the threshold pressure and threshold pressure gradient of the core. Some researchers believe that it is very difficult to observe the movement of a liquid in a capillary tube. Therefore, the flow of the fluid in the core is determined by recording the unit scale displacement of the liquid level. When the liquid level is displaced, the pump is stopped, and the inlet valve is closed. Finally, the minimum threshold pressure is obtained via the balance method, i.e. when the liquid level in the capillary no longer moves and the precision meter reading

is unchanged, the instrument pressure value is read at this time. This is the minimum threshold pressure of this core.

(2) Numerical experiments

The mathematical model involves indirectly solving the minimum threshold pressure gradient by considering various factors that affect the threshold pressure gradient and then establishing mathematical equations. V. Kadet and D. Polonsky studied the correlation between the macro minimum threshold pressure gradient and the micro-media heterogeneity parameters by considering the graduality of the macroscopic flow law at large and small rates. The Bingham plastic nonlinear seepage law that considers the inertia loss is designed to determine the minimum threshold pressure gradient for non-Newtonian fluid displacement. Chai Zhenhua proposed a method based on the lattice Boltzmann method to study nonlinear seepage. The lattice Boltzmann method originates from the lattice gas automaton, which is essentially different from the macroscopic computational fluid dynamics method based on continuous differential equations. According to the fluid microscopic model and the microscopic theoretical equation, the method is not subject to continuous assumptions. Based on the pore properties and capillary pressure effects of porous media, Meijuan Yun proposed an irregular model for the threshold pressure gradient of a Bingham fluid in porous media. Each parameter in the model has a clear physical meaning, and this model relates the structural parameters of the porous medium, the yield stress, the capillary pressure parameter, and the fractal dimension of the porous medium to the threshold pressure gradient of the Bingham fluid.

(3) Well test interpretation

According to the experience of their predecessors, Liu et al. proposed a well test interpretation method to solve the problem of the threshold pressure gradient. The model was established by proposing different control equations, flow velocity equations and internal and external boundary conditions from conventional reservoirs. The well test interpretation method is an on-site dynamic and in-situ test that dynamically reflects the change law of the reservoir. Therefore, the starting pressure gradient determined by the well test method has positive practical significance.

(4) Other

Xu Demin et al. proposed a 'secondary average method' and an improved 'three-time average method' to estimate the proposed pressure gradient according to the seepage characteristics of the non-Darcy flow linear segment. First, the measured value of the measured permeability coefficient is uniformly adjusted, and then the absolute permeability coefficient value is determined. Then, the K value is determined according to the value, and the method of estimating the pressure gradient to be started is calculated by the average of three times.

4. APPLICATION OF THE THRESHOLD PRESSURE GRADIENT

(1) Determination of reasonable well spacing

The impact of the pressure gradient on flooding in conventional heavy oil reservoirs is mainly due to the increase in the seepage resistance and the reduction in the flow capacity of the fluid in the medium, thus significantly reducing the effective range of the flooding. Based on the distribution characteristics of the seepage field under typical injection and production conditions, conditions for effective flooding are proposed, and a method for calculating the effective injection-production well spacing of water flooding in common heavy oil reservoirs has been established. Based on the determined considerations, Zhang Junting proposed the pressure gradient directional well productivity formula, which is based on the micro-element idea and determined the reasonable well spacing and reasonable production capacity of the directional wells. Moreover, based on this method, a reasonable productivity chart and a reasonable well spacing chart of the directional wells under different formation crude oil viscosities were drawn.

(2) Determination of the capacity

Compared with conventional seepage, the existence of a threshold pressure gradient intensifies the pressure drop in the near-well zone, making the 'pressure drop funnel' on the image smaller and sharper and the pressure gradient at the same position larger. In a conventional seepage situation,

the pressure distribution curve and the original formation pressure level is asymptotically tangent, there is no pressure disturbance on the outside edge, and the threshold pressure gradient involves circumstances in which the pressure distribution curves intersect with the horizontal line to show the original formation pressure. Additionally, the crossing angle increases with an increase in the threshold pressure gradient and the pressure disturbance on the outside edge and can be then divided into the flow area and non-current area.

We considered the characteristics of non-Darcy seepage of heavy oil, ignoring the effects of capillary force and gravity and proposed a single well stable seepage productivity formula that includes the influence of the threshold pressure. The higher the threshold pressure gradient, the lower the production per well. When the threshold pressure gradient is relatively large, the seepage resistance increases, and when the pressure difference is small, the crude oil does not flow. With an increase in the pressure difference, the crude oil overcomes the seepage resistance and begins to flow, thus increasing the production of a single well. Moreover, an excessive increase in the pressure difference can easily lead to closure of fractures and holes in the reservoir. Therefore, a reasonable production pressure difference should be considered in the actual production of oilfields.

5. CONCLUSION

This paper summarizes the mechanism of the starting pressure gradient in porous media of heavy oil reservoirs, the measurement method for the starting pressure in two-phase porous media, the numerical simulation studies of starting pressure, the progress in the field study of the starting pressure gradient, and the current research progress and existing issues. Additionally, the application of the starting pressure gradient in oilfield development is reviewed. For a single-phase fluid, the initial pressure gradient is mainly caused by the interaction between crude oil macromolecules. For a two-phase fluid, the mechanism of the starting pressure gradient is mainly the capillary force and viscous resistance. Currently, the method used to measure the starting pressure gradient in the laboratory is primarily the seepage curve fitting method based on the fitting seepage curve. The unsteady state seepage process has been established. The capillary equilibrium method based on the principle of the communicator. In field application, the start-up pressure gradient has a significant effect on well pattern spacing and well production. To study the start-up pressure gradient of heavy oil reservoirs, it is necessary to start with the properties of crude oil and its pore structure. Understanding the mechanism of the start-up pressure gradient in heavy oil reservoirs is of considerable significance to the actual production and development of oil fields and the oil and water migration in porous media.

REFERENCES

- [1] Ding J , Yang S , Cao T , et al. Dynamic threshold pressure gradient in tight gas reservoir and its influence on well productivity[J]. *Arabian Journal of Geosciences*, 2018, 11(24).
- [2] Mao X , Liu Y , Guan W , et al. Experimental and numerical simulation on the influence of anisotropic fracture network deformation to shale gas percolation[J]. *Arabian Journal of Geosciences*, 2018, 11(20).
- [3] Xin J , Li C , Chai R . Effect of sulfate ions on oil detachment from calcite surface: experiments and molecular dynamics simulations[J]. 2019.
- [4] Tianyi Z , Xiangfang L , Zhengfu N , et al. Pore structure and adsorption behavior of shale gas reservoir with influence of maturity: a case study of Lower Silurian Longmaxi formation in China[J]. *Arabian Journal of Geosciences*, 2018, 11(13):353-.
- [5] Zhao Z , Ma W , Fu X , et al. Energy theory and application of rocks[J]. *Arabian Journal of Geosciences*, 2019, 12(15).
- [6] Zheng W , Liu Y , Huang J , et al. Study on the optimal development method for offshore buried hill fractured reservoirs[J]. *Arabian Journal of Geosciences*, 2018, 11(20):640.

-
- [7] Khatyr R, Ouldhadda D, Idrissi A. II. Viscous dissipation effects on the asymptotic behavior of laminar forced convection for Bingham plastics in circular ducts. *Int J Heat Mass Transf* 2003;46:589–98.
- [8] Blackery J, Mitsoulis E. Creeping motion of a sphere in tubes filled with a Bingham plastic material. *J Non-Newton Fluid Mech* 1997;70:59–77.
- [9] Roquet N, Saramito P. An adaptive finite element method for Bingham fluid flows around a cylinder. *Comput Methods Appl Mech Eng* 2003;192:3317–41.
- [10] Balhoff MT, Thompson KE. Modeling the steady flow of yield stress fluids in packed beds. *AIChE J* 2004;50:3034–48.
- [11] Prada A, Civan F. Modification of Darcy's law for the threshold pressure gradient. *J Petrol Sci Eng* 1999;22:237–40.
- [12] Chen M, William R, Yannis Yortsos C. The flow and displacement in porous media of fluids with yield stress. *Chem Eng Sci* 2005;60(15):4183–202.
- [13] Wang SJ, Huang YZ, Civan F. Experimental and theoretical investigation of the Zaoyuan field heavy oil flow through porous media. *J Petrol Sci Eng* 2006;50:83–101.
- [14] Yun MJ, Yu BM, Cai JC. A fractal model for the starting pressure gradient for Bingham fluids in porous media. *Int J Heat Mass Transf* 2008;51:1402–8.
- [15] Li Y, Yu BM. Study of the starting pressure gradient in branching network. *Sci. China Tech Sci* 2010;53(9):2397–403.
- [16] Kou JL, Liu Y, Wu FM, Fan JT, Lu HJ, Xu YS. Fractal analysis of effective thermal conductivity for three-phase (unsaturated) porous media. *J Appl Phys* 2009;106:054905-1–5-6.
- [17] Chen YP, Wu R, Shi MH, Wu JF, Peterson GP. Visualization study of steam condensation in triangular microchannels. *Int J Heat Mass Transf* 2009;52:5122–9.
- [18] Barenblatt GE, Zheltov IP, Kochina IN. Basic concepts in the theory of seepage of homogeneous liquids in fissured rocks. *J Appl Math Mech* 1960;24:1286–303.
- [19] Sahimi M. *Flow and transport in porous media and fractured rocks*. Germany, VCH: Weinheim; 1995.
- [20] Yu BM, Cheng P. A fractal permeability model for bi-dispersed porous media. *Int J Heat Mass Transf* 2002;45:2983–93.
- [21] Yu BM, Liu W. Fractal analysis of permeabilities for porous media. *AIChE J* 2004;50:46–57.
- [22] Yu BM. Analysis of flow in fractal porous media. *Appl Mech Rev* 2008;61:050801-1–0Yu BM. Fractal character for tortuous streamtubes in porous media. *Chin Phys Lett* 2005;22:158–60.
- [23] Bird RB, Stewart WE, Lightfoot EN. *Transport phenomena*. New York: Wiley; 1960.

The impact of Al₂O₃ doping in vinyl ester resin on gamma radiation attenuation coefficient

İlyas KARTAL¹, Kadir GÜNOĞLU^{2*}, İskender AKKURT³

¹ Marmara University Technology Faculty Metallurgy and Materials Engineering Department İstanbul-TURKEY

² Isparta University of Applied Sciences, Technical Vocational School, Isparta- TURKEY

³ Suleyman Demirel University, Science Faculty, Physics Department, Isparta-TURKEY

ABSTRACT

With the discovering atomic nucleus, nuclear science started to be used in different fields and researcher focused on radiation protection as it is dangerous for human cell. Thus radiation physics and materials development becomes one of the important subject in science for this purposes. The developed material should be used for radiation shielding. In this study, aluminum oxide particle reinforced vinyl ester composite materials were produced. The radiation shielding performance of the composite materials produced was experimentally measured at 511 keV gamma energy emitted from ²²Na radioactive source.

KEYWORDS - Vinyl ester resin, aluminum oxide, radiation attenuation coefficient

1. INTRODUCTION

There has been increasing interest in gamma irradiation and isotopes, which have been spatially incorporated into medical applications such as sterilisation, radio-pharmaceuticals, radiotherapy and so on extensively [1]. Long-term exposure to gamma irradiation can have dangerous effects on human health, including cancer and death, which is the reason there has been a growing interest in finding ways to protect humans from such exposure. In the past decade, significant emphasis has been placed on developing smart and efficient radiation shielding materials [2,3]. Such shielding materials eliminate the hazard dosage of radiation by interacting with the radiation itself, leading to the decrease or complete elimination of its power.

Metals such as lead, tungsten and bismuth have high densities and high atomic weights. Thus, their composites are applied to decrease the hazard dosage of radiation [4]. Moreover, the high atomic weights of metals with polymer composites are more applicable, less toxic, heavy, highly mechanical, chemically stable, flexible [5] and low cost, in addition to its ability to achieve mimic unique properties depending on the methods of preparation [6-8]. Such high-performance polymeric composites, including epoxies, polyimides, polybenzimidazoles and polyester [9,10], have high mechanical and thermal properties, good durability, in conjunction with hole-free structures and compactness. The promising thermosetting vinyl ester (VE) monomer is a very common matrix in terms of the reinforcing composites owing to its low price and easy processability.

In this study, aluminum oxide particle reinforced vinyl ester composite materials were produced. The radiation shielding performance of the composite materials produced was experimentally measured at 511 keV gamma energy emitted from ²²Na radioactive source.

2. MATERIAL AND METHOD

2.1. Sample preparation

In the process of adding aluminum oxide to the vinyl ester resin, 2% by weight was added. After this rate, the resin was unable to wet the aluminum oxide (Al₂O₃) supplement. For example, in the sample preparation process for the sample containing 0.5% boron nitride by weight, first of all, aluminum oxide particles were mixed with an ultrasonic mixer for 30 minutes in MEG (mono ethylene glycol) at a ratio of 5 times the particle amount in order to ensure homogeneous distribution and to prevent clumping. Vinyl ester resin was placed in a container. Aluminum oxide dispersed in MEG in the ratio of 0.5% by weight of the total amount to be formed was added into the resin and

mixing was applied with a mechanical mixer for about 10 minutes. After mixing, 3% active methyl ethyl ketone peroxide was added as hardener at a rate of 3%, and after it was mixed thoroughly, 1% cobalt naphthalate was added as accelerator and mixed again. After ensuring a homogeneous mixture, the mixture was poured into the silicone mold that was placed on a smooth surface and balanced with a water balance. The silicone mold was kept at 85 ° C for 10 minutes and the cured samples were removed from the mold.

2.2. EXPERIMENTAL PROCEDURE

The gamma ray attenuation coefficient of composite material have been performed using the gamma spectrometer, containing a 3” × 3” inch sodium iodide with thallium (NaI (Tl) detector, coupled to a digital spectrum analyzer (DSPEC LF), connected to the 16k channels Multi Channel Analyzer (MCA) provided by ORTEC hardware, controlled by MAESTRO32 software (Figure 1).

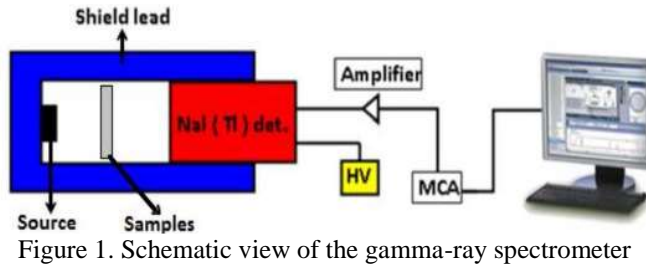


Figure 1. Schematic view of the gamma-ray spectrometer

The gamma ray attenuation coefficients μ (cm-1) is obtained by:

$$\mu = \frac{1}{x} \ln \frac{I_0}{I} \tag{1}$$

where x is the material thickness and I and I0 are the background subtracted number of counts recorded in detector with and without material between detector and source, respectively.

3. RESULTS AND DISCUSSION

The linear ray attenuation coefficient for 2% aluminum oxide (Al₂O₃) particle reinforced vinyl ester resin composite material was measured using a gamma spectrometer for 511 keV gamma energy. The results obtained are shown in Figure 2.

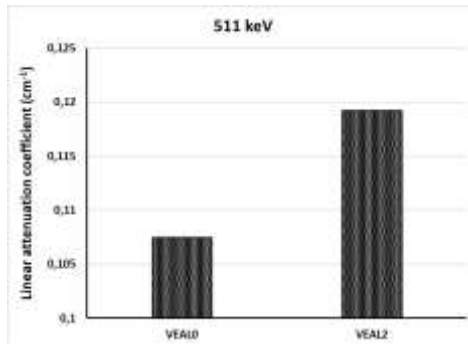


Figure 2. Results of gamma ray attenuation coefficient

As seen in Figure 2, the vinyl ester resin composite material aluminum oxide (Al_2O_3) particle reinforcement increased the linear attenuation coefficient.

REFERENCES

- [1].Singh, J., Singh, H., Sharma, J., Singh, T., Singh, P.S., 2018. Fusible alloys: a potential candidate for gamma rays shield design. *Prog. Nucl. Energy* 106, 387–395.
- [2].Kaur, T., Sharma, J., Singh, T., 2019. Experimental evaluation of gamma rays shielding parameters for Zn-Cd-Sn-Pb quaternary alloy. *Radiat. Phys. Chem.* 156, 193–198.
- [3].Kaur, P., Singh, D., Singh, T., 2018. Gamma rays shielding and sensing application of some rare earth doped lead-alumino-phosphate glasses. *Radiat. Phys. Chem.* 144, 336–343.
- [4].Vaz, P., 2015. Radiological protection, safety and security issues in the industrial and medical applications of radiation sources. *Radiat. Phys. Chem.* 116, 48–55.
- [5].Mahmoud, M.E., El-Khatib, A.M., Badawi, M.S., Rashad, A.R., El-Sharkawy, R.M., Thabet, A.A., 2018. Fabrication, characterization and gamma rays shielding properties of nano and micro lead oxide-dispersed-high density polyethylene composites. *Radiat. Phys. Chem.* 145, 160–173.
- [6].Valles, C., Abdelkader, A.M., Young, R.J., Kinloch, I.A., 2015. The effect of flake diameter on the reinforcement of few-layer graphene–PMMA composites. *Compos. Sci. Technol.* 111, 17–22.
- [7].Issa, S.A.M., Sayyed, M.I., Zaid, M.H.M., Matari, K.A., 2018. Photon parameters for gamma-rays sensing properties of some oxide of lanthanides. *Results Phys.* 9, 206–210.
- [8].Kacal, M.R., Akman, F., Sayyed, M.I., 2018. Investigation of radiation shielding properties for some ceramics. *Radiochim. Acta.*
- [9].Lin, Z.-I., Lou, C.-W., Pan, Y.-J., Hsieh, C.-T., Huang, C.-H., Huang, C.-L., Chen, Y.-S., Lin, J.-H., 2017. Conductive fabrics made of polypropylene/multi-walled carbon nanotube coated polyester yarns: mechanical properties and electromagnetic interference shielding effectiveness. *Compos. Sci. Technol.* 141, 74–82.
- [10]. Li, Y., Shen, B., Yi, D., Zhang, L., Zhai, W., Wei, X., Zheng, W., 2017. The influence of gradient and sandwich configurations on the electromagnetic interference shielding performance of multilayered thermoplastic polyurethane/graphene composite foams. *Compos. Sci. Technol.* 138, 209–216.

Experimental Study on the Effect of Key Ions in Smart Water Flooding for Carbonate Reservoirs in Middle East

Songqi LI1, Yuetian LIU1* ,Wenli KE2, Jun LI1,

1 State Key Laboratory of Petroleum Resources and Prospecting, China University of Petroleum (Beijing),
Beijing 102249, China

2 Yangtze University, College of Petroleum Engineering, Wuhan, China

* Yuetian Liu @institution.org

ABSTRACT

For many decades, smart water flooding has been used to improve oil recovery in carbonate reservoirs, but in the last few years, research showed some inefficiencies in the use of this method, such as failure to give an incremental oil recovery. In this study, insights on oil recovery caused by Mg^{2+} and SO_4^{2-} were made by investigating the effects of ions on rock/fluids and fluid/fluid interactions. Mg^{2+} and SO_4^{2-} were shown to improve the oil recovery in carbonate reservoir. With the increase in Mg^{2+} concentration from 874 mg/L to 8740 mg/L, there was an appreciable increase in oil recovery from 60% to 79%, the contact angle changed from 95% to 83.1%, and the zeta potential increased from 2.11 mv to 5.82 mv. On the other hand, with the increase in SO_4^{2-} concentration from 558 mg/l to 12705 mg/l, there was an appreciable increase in oil recovery from 58% to 72%, the contact angle decreased from 95° to 85°, and the zeta potential decreased from 5.82 mv to -31.2 mv. It can be seen that although Mg^{2+} and SO_4^{2-} improved the oil recovery in carbonate reservoir, SO_4^{2-} improved oil recovery more than Mg^{2+} .

KEYWORDS - carbonate reservoir, low salinity water flooding, oil recovery, oil chemistry, experimental study

1. INTRODUCTION

Carbonate reservoirs are reported to contain almost half of the world hydrocarbon proven reserves, and 90% of them are observed to be mixed-wet to oil-wet. After the primary and secondary recovery stages of the life cycle of the field, reasonable amounts of residual oil are still left in the reservoir. Till date, one of the most economical and efficient EOR techniques for carbonate reservoirs is smart water flooding[1, 2] because it only needs to adjust the composition of injected water, without any improvement of ground facilities.

It is generally believed that oil recovery can be improved by smart water flooding, but there exists apparent disagreement between the results and conclusion in these studies because of the different experimental conditions[3-7]. As a result, different people hold different points about the mechanisms behind the smart water flooding, for example, in double-layer expansion, particle migration, mineral dissolution and in situ reaction to form complexes, among others. H.H.Al-Attar, M.Y.Mahmoud carried out flooding tests on carbonate which indicated that oil recovery increased from 63% to 84.5% and the zeta potential decreased as the salinity decrease from 196,362 ppm to 5000 ppm.[8] The potency of smart water to improve oil recovery has higher potential compared to the conventional water flooding[9-10]. Laboratory water flooding experiment and successful field trials have shown that smart water flooding can improve the oil recovery in sandstone reservoirs. On the other hand, although considerable progress has been made, particularly in the last 5 years, this has been accompanied by much debate, and some unexpected and intriguing findings have emerged. Skrettingland reported no change in ROS around the wellbore on a field trial at the formation. The Snorre field case is among a few reported cases where this emerging concept has failed to give an incremental oil recovery[11]. With recent development following a paradigm shift in carbonate reservoirs, an experimental success reported for carbonate weakened the argument that smart water will not improve oil recovery in carbonate due to the absence of clay minerals which is considered a key prerequisite for smart water flooding application. Both salinity and water ions

affect the chemistry of injection water. Many studies showed that certain ions, such as Ca^{2+} , Mg^{2+} and SO_4^{2-} , play a major role in affecting oil recovery in carbonates. Hasan and his coworkers study the impact of Ca^{2+} , Mg^{2+} and SO_4^{2-} on wettability by core flooding experiments, and they reported that oil recovery increases as the content of key ions increase[12].

2. EXPERIMENTAL

1) Material

The carbonate cores used in this study were taken from the Missan reservoir in the Middle East. Dead crude oil from the Missan reservoir in the Middle East and synthetic formation brine were used in this study. In this study, the formation of water components measured in the field are shown in Table 1.

Table1. Different smart water components

Composition	Na ⁺ (mg/L)	Ca ²⁺ (mg/L)	Mg ²⁺ (mg/L)	K ⁺ (mg/L)	HCO ³⁻ (mg/L)	SO ₄ ²⁻ (mg/L)	Cl ⁻ (mg/L)	salinity (mg/L)
FW	37504.80	6813.40	874.00	585.45	211.35	558.35	72567.45	119230.25
1-Mg ²⁺	7863.94	1428.62	183.26	122.76	44.32	117.07	15215.82	25000.00
2-Mg ²⁺	7634.04	1428.62	364.58	122.76	44.32	117.07	15357.62	25069.01
3-Mg ²⁺	7220.22	1428.62	607.63	122.76	44.32	117.07	15428.52	24969.14
4-Mg ²⁺	6392.58	1428.62	1154.49	122.76	44.32	117.07	15747.57	25007.41
1-SO ₄ ²⁻	7938.66	1428.62	183.26	122.76	44.32	240.00	15215.82	25173.44
2-SO ₄ ²⁻	7881.19	1428.62	183.26	122.76	44.32	480.00	14949.95	25090.09
3-SO ₄ ²⁻	7846.70	1428.62	183.26	122.76	44.32	960.00	14542.27	25127.93
4-SO ₄ ²⁻	7823.71	1428.62	183.26	122.76	44.32	1440.00	14152.32	25194.99

2) Contact Angle Measurement Experiment

The wetting angle measurement works were performed to study the effects of the salinity and the composition of injected brine on the wettability of carbonate surface.

3) Zeta electroacoustic spectrometer Experiment

Zeta electroacoustic spectrometer was applied to measure the zeta potential for rock/brine interface.

4) Results

The effect of key ions on oil recovery

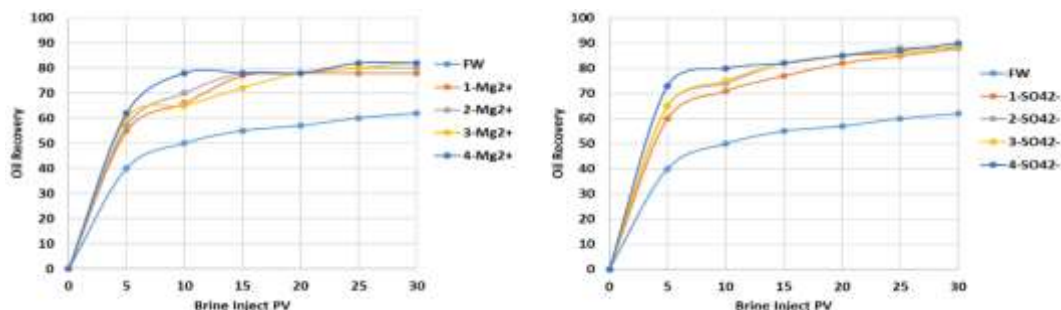


Figure 1. Oil recovery vs different injected brine with Mg²⁺ and SO₄²⁻

The effect of key ions on contact angle

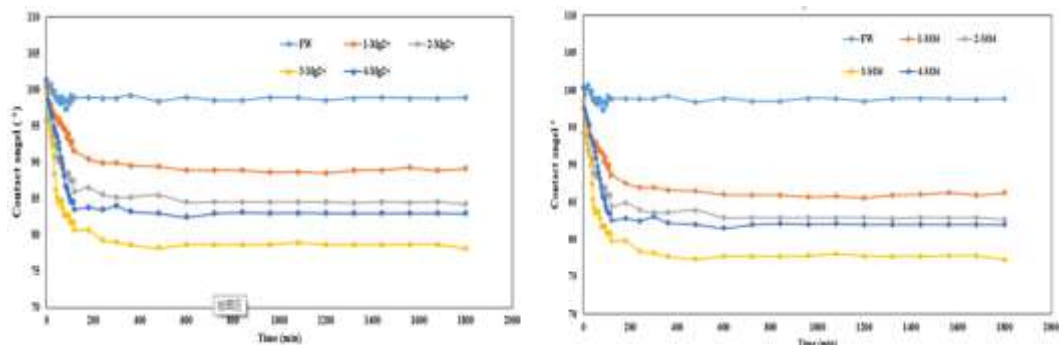


Figure 2. The mechanism of magnesium for Mg²⁺ and SO₄²⁻

The effect of key ions on zeta potential

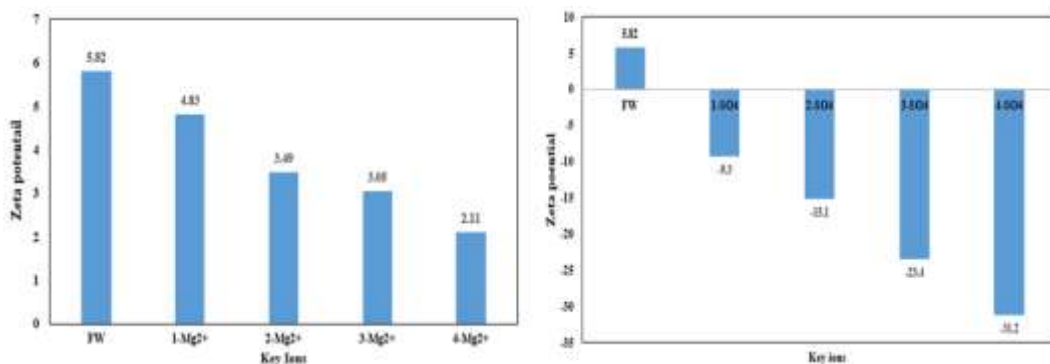


Figure 3. The mechanism of zeta potential for Mg²⁺ and SO₄²⁻

Firstly, the oil recovery increased from 56% to 97%, the contact angle changed from 95° to 83.1°, and the zeta potential increased from 2.11 mV to 5.82 mV, as the Mg²⁺ concentration increased from 874 mg/L to 8740 mg/L. Consequently, even if the Mg²⁺ concentration continued to increase, the oil recovery would not change significantly. On the other hand, the oil recovery increased from 58% to 72%, the contact angle decreased from 95° to 85°, and the zeta potential decreased from 5.82 mV to -31.2 mV, as SO₄²⁻ concentration increased from 558 mg/L to 12705 mg/L. The oil recovery results by displacement experiments showed a noticeable improvement by switching to the Mg²⁺ concentration, and SO₄²⁻ has more effect than Mg²⁺ on the oil recovery. Results of contact angle study showed that due to the increase of Mg²⁺ and SO₄²⁻, wettability alteration towards more water-wet condition occurred in this study. Zeta potential measurements showed that increasing Mg²⁺ and SO₄²⁻ can change the potential appreciably.

3. CONCLUSION

In this study, the mechanisms behind the effect of Mg²⁺ and SO₄²⁻ on oil recovery were carried out. It was found that the oil recovery results by displacement experiments showed a noticeable improvement by switching to the Mg²⁺ concentration and that SO₄²⁻ had more effect than Mg²⁺ on oil recovery. Results of contact angle study showed that due to the increase of Mg²⁺ and SO₄²⁻, wettability alteration towards more water-wet condition occurred in this study. The zeta potential measurements showed that increasing Mg²⁺ and SO₄²⁻ can change the potential appreciably. In this study, observations proved that Mg²⁺ and SO₄²⁻ will change the wettability and potential, which can be the main mechanism contributing to oil recovery enhancement.

REFERENCES

- [1] Li S, Liu Y, et al. An investigation on water flooding performance and pattern of porous carbonate reservoirs with bottom water. *J. Petrol. Sci. Eng.* Volume 200, ISSN 0920-4105. <https://doi.org/10.1016/j.petrol.2021.108353>.
- [2] Wang H, Tian L, Gu D, et al. Method for Calculating Non-Darcy Flow Permeability in Tight Oil Reservoir[J].*Transport in Porous Media.* 2020, 133. <https://doi.org/10.1007/s11242-020-01427-8>.
- [3] Chavan M, Dandekar A, Patil S. et al. Low-salinity-based enhanced oil recovery literature review and associated screening criteria. *Pet. Sci.* 16, 1344–1360 (2019). <https://doi.org/10.1007/s12182-019-0325-7>
- [4] Joel T. T, Patrick V. B, Reza Barat Ghahfarokhi. Review of low salinity water flooding in carbonate rocks: mechanisms, investigation techniques, and future directions. *Advances in Colloid and Interface Science.* Volume 284 (2020), ISSN 0001-8686. <https://doi.org/10.1016/j.cis.2020.102253>.
- [5] Mohammadi M , Mahani H . Direct Insights into the Pore-scale Mechanism of Low Salinity Water flooding in Carbonates Using a Novel Calcite Microfluidic Chip. *Fuel.* Volume 260(2020), ISSN 0016-2361. <https://doi.org/10.1016/j.fuel.2019.116374>.
- [6] Sun L, Li Y, et al (2019). Water-Out Performance and Pattern of Horizontal Well for a Thin Carbonate Reservoir with Bottom Water in the Middle East. *Offshore Technology Conference Brasil, Rio de Janeiro, Brazil, October 2019. SPE-29709-MS.* <https://doi.org/10.4043/29709-MS>.
- [7] Miku T, Mai S, Yogarajah E, et al. Predicting the electro kinetic properties of the crude oil/brine interface for enhanced oil recovery in low salinity water flooding. *Fuel* Volume 235(2019), ISSN 0016-2361. <https://doi.org/10.1016/j.fuel.2018.08.079>.
- [8] Aldousary S, Kovscek A R. The diffusion of water through oil contributes to spontaneous emulsification during low salinity water flooding. *J. Petrol. Sci. Eng.* Volume 179(2019), ISSN 0920-4105. <https://doi.org/10.1016/j.petrol.2019.04.041>.
- [9] Joel T. T, Patrick V. B, Reza Barat Ghahfarokhi. Review of low salinity water flooding in carbonate rocks: mechanisms, investigation techniques, and future directions. *Advances in Colloid and Interface Science.* Volume 284 (2020), ISSN 0001-8686. <https://doi.org/10.1016/j.cis.2020.102253>.
- [10] Ghandi E, Parsaei R. & Riazi M. Enhancing the spontaneous imbibition rate of water in oil-wet dolomite rocks through boosting a wettability alteration process using carbonated smart brines. *Pet. Sci.* 16, 1361–1373 (2019). <https://doi.org/10.1007/s12182-019-0355-1>
- [11] Mohammadi M , Mahani H . Direct Insights into the Pore-scale Mechanism of Low Salinity Water flooding in Carbonates Using a Novel Calcite Microfluidic Chip. *Fuel.* Volume 260(2020), ISSN 0016-2361. <https://doi.org/10.1016/j.fuel.2019.116374>.
- [12] Yamin W, Muhan Y, et al. Effect of temperature on mineral reactions and fines migration during low salinity water injection into Berea sandstone. *J. Petrol. Sci. Eng.* Volume 202(2021), ISSN 0920-4105. <https://doi.org/10.1016/j.petrol.2021.108482>.

Behavior of some ceramic materials against gamma ray with 662 keV energy

Mohammed A.M. ALNASER^{1*}, Kadir GÜNOĞLU², Nermin DEMİRKOL³ İskender AKKURT¹

1 Suleyman Demirel University, Science Faculty, Physics Department, Isparta-TURKEY

2 Isparta University of Applied Sciences, Technical Vocational School, Isparta- TURKEY

3 Kocaeli University, Faculty of fine arts, Ceramic Department, Isparta-TURKEY

ABSTRACT

With the advancement in science and technology, nuclear technology is being employed in many field such as energy, food, agriculture, medicine and industry. The importance of radiation shielding and protection is more and more increasing in parallel with the enlargement of the application areas of nuclear technology. Therefore, studies on the shielding properties of different materials have already been performed. Regarding alternatives to conventional radiation prevention methods such as lead, heavy concrete amongst others, focus on other functional materials are necessary. Some ceramic materials are used to study gamma-ray shielding properties. The transmitted fluxes of gamma-ray that was emitted from ¹³⁷Cs source was detected by a NaI(Tl) detector and analyzed by a MCA analyzer. Then, linear attenuation coefficients were experimentally investigated.

Keywords: ceramic material, gamma ray, NaI(Tl) detector, linear attenuation coefficient

1. INTRODUCTION

Ceramic entered within building materials and used in different applications such as mechanical applications, electrical and magnetic applications, nuclear power, etc. Ceramics are composite materials that have mechanical properties such as strength, toughness, wear resistance, high melting point and hardness [1]. Ceramic is defined as a solid, complex and difficult material; this material is characterized by many properties including durability, toughness and hardness, chemical reaction, lack of porosity, limited risk and contamination and the flexibility of formation.

With the increasing use of gamma radiation in various applications in industry, medicine, agriculture, nuclear reactors and particle accelerators, the exposure for longer duration to these radiations can cause very harmful effects on human health. It must be protected against the radiation; the fundamental principle of radiation protection is to minimize exposure to radiation; it is possible to employ three main principles by reducing time, increase the distance and shielding between the source and personnel.

Therefore, the usage of shielding becomes of a paramount importance for using this radiation without a risk [2]. Lead usually uses to protect from gamma ray because it has a high density (high atomic number). Various researches concerning the interaction and shielding of gamma-rays for such as ceramic, concrete, barite, marble and limra instead of lead have been published in literature [2–8] and such studies are still actual.

In the present study, the linear attenuation coefficient (LAC) for White Mud (WM) and Slide Casting Mud (SCM) ceramic samples has been measured by using a gamma-ray spectrometer and ¹³⁷Cs radioactive gamma source (emitted gamma with 662 keV energy).

2. MATERIAL AND METHOD

All samples were prepared in the same way which firstly prepared the material then start knead the clay and rolling well by pushing it down and away, strongly by hand to empty the air bubbles from the material. This kneading for clay continues for at least two minutes. Air bubbles can make the material broken when sintering it, so get them out before start working. The materials put in the mold, also pressed several times by hand until the material takes the shape of the mold after that

extract the material from the mold and left it for some time under room temperature to dry. Each sample placed in the kiln under 950°C for 8 hours to sintering ceramic samples.

LAC of ceramic samples were measured to determine their gamma ray shielding properties using a low level gamma counting spectroscopy system containing a NaI (Tl) detector. Gamma spectroscopy system consists of electronic parts such as High Voltage (HV), Amplifier, Multi-Channel Analyzer (MCA). The experiments were performed at 662 keV gamma ray which was obtained from 137Cs radioactive source.

As a result of the interaction of gamma rays with matter, some of the rays are absorbed, some of them are transmitted directly without interaction and some of them are scattered in different directions. The realization of these interactions depends on the properties of the shield material, the incoming gamma energy and the measurement geometry. In order for the results of the experimental measurements to be accurate, an ideal experimental geometry called narrow beam geometry was created. The electronic components and geometry of the gamma counting spectroscopy system used in this study are shown in Figure 1. The multi-channel analyzer in the system creates spectra with digital signal processing techniques and the areas of these obtained spectra are calculated using MAESTRO-32 software.

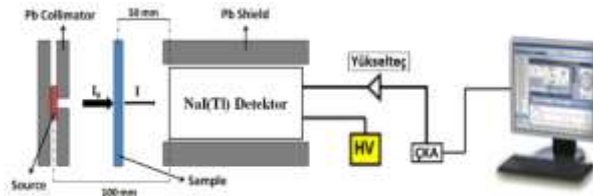


Figure 1. The electronic components and geometry of the gamma counting spectroscopy system

The linear attenuation coefficients (μ) are measured by the following equation:

$$N = N_0 e^{-\mu x}$$

where μ is linear attenuation coefficient (cm^{-1}); N is the number of photons detected by the detector during a specified period of time when a material with a determined thickness (x) is placed between the source and the detector; N_0 is the number of photon source without material.

3. RESULTS AND DISCUSSION

The linear attenuation coefficients for White Mud (WM) and Slide Casting Mud (SCM) have been measured using gamma spectrometer for 662 keV gamma energy. The obtained results are shown in Figure 3.

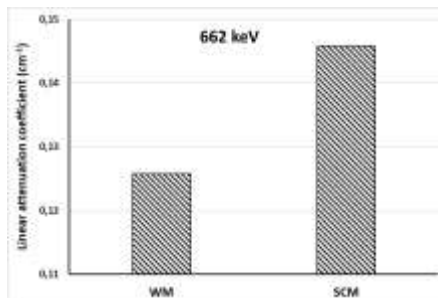


Figure 3. Results of linear attenuation coefficient

As seen in Figure 3, the linear attenuation coefficient of Red Mud was measured higher than Kütahya Tile Mud. It can be said that the results obtained vary depending on the chemical content and density of the materials.

REFERENCES

- [1]. Ceramics (2017) Chemistry encyclopedia. <http://www.chemistryexplained.com/Bo-e/Ceramics.html>.
- [2]. Y. Elmahroug, B. Tellili, C. Souga, Determination of total mass attenuation coefficients, effective atomic numbers and electron densities for different shielding materials *Ann. Nucl. Ener.* 75, 268 (2015).
- [3]. Akkurt I, Elkhayat A (2013) The effect of barite proportion on neutron and gamma-ray shielding. *Ann Nucl Energy* 51:5–9
- [4]. Akkurt I, Basyigit C, Kilincarslan S (2004) The photon attenuation coefficients of barite, marble and limra. *Ann Nucl Energy* 31(5):577–582
- [5]. Akkurt I, Basyigit C, Kilincarslan S, Mavi B (2005) The shielding of γ -rays by concretes produced with barite. *Prog Nucl Energy* 46(1):1–11
- [6]. M.T. Teli, L.M. Chaudhari, S.S. Malode, Attenuation coefficients of 123 keV γ -radiation by dilute solutions of sodium chloride *Appl. Ra-diat. Isotopes* 45, 987 (1994).
- [7]. K. Singh, H. Singh, V. Sharma, R. Nathuram, A. Khanna, R. Kumar, S.S. Bhatti, H.S. Sahota, Gamma-ray attenuation coefficients in bismuth borate glasses, *Nucl. Instr. Methods B* 194, 1 (2002).
- [8]. I. Akkurt, K. Gunoglu, S.S. Arda, Detection Efficiency of NaI(Tl) Detector in 511–1332 keV Energy Range *Sci. Technol. Nucl. Install.* 2014, 186798 (2014).
- [9]. Akkurt I, Basyigit C, Mavi B, Kilincarslan S, Akkurt A (2006) Radiation shielding of concretes containing different aggregates. *Cem Concr Compos* 28(2):153–157
- [10]. Akkurt I, Mavi B, Kilincarslan S, Basyigit C, Akyıldırım H (2009) Investigation of photon attenuation coefficient for pumice. *Int J Phys Sci* 4(10):588–591
- [11]. Akkurt I et al (2010) Photon attenuation coefficients of concrete includes barite in different rate. *Ann Nucl Energy* 37:910–914
- [12]. Al-Sarray E, Akkurt I, Günoğlu K, Evcin A, Bezir NÇ (2017) Radiation shielding properties of some composite Panel. *Acta Phys Polon A* 132(3):490–492

Experimental Study on Chemistry of Produced Oil in Carbonate Reservoirs During High- and Low-Salinity Water Flooding

Songqi LI1, Yuetian LIU1* ,Wenli KE2, Jun LI1,

1 State Key Laboratory of Petroleum Resources and Prospecting, China University of Petroleum (Beijing),
Beijing 102249, China

2 Yangtze University, College of Petroleum Engineering, Wuhan, China

* Yuetian Liu @institution.org

ABSTRACT

The potential of low-salinity water flooding as an oil recovery technique has attracted great attention in the petroleum industry. This study presents an investigation on how low-salinity water affects oil recovery and chemistry of produced oil in carbonate reservoirs during low-salinity water flooding. The core displacement experiments and the Fourier-transform infrared spectroscopy (FTIR) were carried out to study the impact on the chemistry and composition of the oil recovered. The results showed that oil recovery increased with the decrease of salinity. Fourier-transform infrared spectroscopy experiments showed that there was an obvious increase in the—COOH as salinity decreased. The primary goal of this work is to understand the effects of salinity on oil recovery and the chemistry of oil production. The results will provide a novel insight into the water–oil interactions in carbonate reservoirs during low-salinity water flooding.

KEYWORDS - carbonate reservoir, low-salinity water flooding, oil recovery, oil chemistry, experimental study

1. INTRODUCTION

Low-salinity water flooding is an economical and efficient oil field development technology, which can reverse the wettability of the oil reservoir and transform it from an oil-wet increase to a water-wet reservoir[1-5]. Significant research efforts have been presented to modify the chemistry of produced oil in carbonate reservoirs during low-salinity water flooding. It is generally accepted that oil recovery can be improved during secondary or tertiary water flooding by controlling the composition of the injected water[6]. With the growing interest in low-salinity water flooding, several mechanisms have been proposed. However, these proposed mechanisms were based on the chemistry property of the injected water and differences in surface wettability in the presence of the low-salinity water flooding.

Mechanisms that reveal the effect of chemistry of low-salinity water on crude oil have not yet been realised[7]. It remains challenging to study the interaction between the oil and water interface, whereby in spite of all these studies, the mechanism in low-salinity water flooding is still unclear. Researchers basically consider only the chemical reactions between water phase salinity, key ions in water phase and rocks and minerals, but they do not often study the mechanism of oil–water rock interface properties due to the active components in crude oil[8].

This study presents an investigation on how low-salinity water affects oil recovery and the chemistry of oil produced in carbonate reservoirs during low-salinity water flooding[9]. The core displacement experiments with the formation of brine and various versions of diluted formation water were carried out to study the influence of salinity on oil recovery. After that, the produced oil and effluent brine were collected and analysed using Fourier-transform infrared spectroscopy (FTIR) which essentially measures the functional group and studies the impact on the nature and composition of the oil recovered[10].

The results of core displacement experiments showed that the oil recovery increased with a decrease in salinity, which demonstrated the role of salinity in oil recovery. Fourier-transform infrared spectroscopy experiment showed that there was an obvious increase in the—COOH as salinity decreased. The primary goal of this work is to understand the effects of salinity on oil recovery and

chemistry. The results will provide a novel insight into the water–oil interactions in carbonate reservoirs during low-salinity water flooding.

2. EXPERIMENTAL

2.1 Material

Artificial carbonate core made by cementing compaction process was used in the experiment. The physical property is controllable, and the lithology is uniform. The experiment was completed by using simulated formation water with distilled water, simulated low-salinity water and surface degassed crude oil from the carbonate reservoir.

2.2 Low-salinity water flooding experiment of long carbonate core

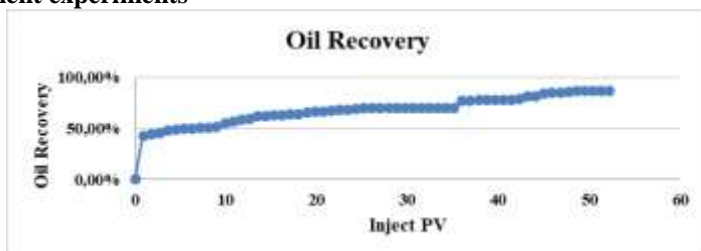
A group of carbonate long-core displacement experiments were carried out in the experiment. The water injection scheme involves the transfer from high-salinity water to low-salinity water –1 to low-salinity water –2. The displacement temperature was 60°C, the flow rate was 0.1 ml /min, the saturation of high-salinity bound water was 20%, and the reservoir aged for 2 weeks under the pressure of displacement temperature.

2.3 Fourier-transform infrared spectroscopy

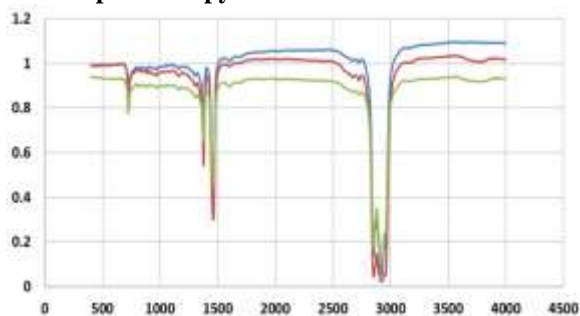
Will get the high-salinity extraction oil displacement experiment produced oil, low salinity, low salinity - 1-1-2 let stand extraction oil, low salinity produced oil, low salinity - 2 let stand extraction oil spectrum experiments, respectively named save experimental data produced oil spectrum of high-salinity results produced oil spectrum, low salinity - 1-1 let stand, low salinity produced oil spectrum results, low salinity - 2 extraction oil spectrum, low salinity - 2 let stand extraction oil spectrum results.

2.4 Results

Core displacement experiments



Fourier-transform infrared spectroscopy



2.5 Discussion

The results of core displacement experiments showed that the oil recovery increased with the decrease of salinity, demonstrating the role of salinity in oil recovery. Fourier-transform infrared spectroscopy experiments showed that there was an obvious increase in the –COOH as salinity decreased. The primary goal of this work was to understand the effects of salinity on oil recovery

and the chemistry of oil production. The results will provide a novel insight into the water–oil interactions in carbonate reservoirs during low-salinity water flooding.

3. CONCLUSION

The significance of this paper is to study the effect of polar composition of crude oil in oil recovery during low-salinity water flooding in carbonate reservoir and to identify the suitability of low-salinity water flooding from the perspective of crude oil composition. The study on the effect of crude oil components on oil recovery during low-salinity water flooding in carbonate reservoirs is still in its early stage; thus, the research results from this study show both theoretical and practical significance.

REFERENCES

- [1] Xiaolong, Mao, Yuetian, et al. Experimental and numerical simulation on the influence of anisotropic fracture network deformation to shale gas percolation[J]. ARABIAN JOURNAL OF GEOSCIENCES, 2018. Doi: 10.1007/s12517-018-3973-9
- [2] Zhang L , Zhou F , Mou J , et al. Research on sensitivity damage of naturally fractured carbonate reservoirs in Ordos Basin[J]. Arabian Journal of Geosciences, 2019, 12(18). DOI : 10.1007/s12517-019-4805-2
- [3] Duan L , Xia Z , Qu L , et al. A new approach of history matching coalbed methane pilot wells[J]. Arabian Journal of Geosciences, 2019, 12(16):1-7. DOI : 10.1007/s12517-019-4619-2
- [4] Liang, Huang, Zhengfu, et al. Enhanced gas recovery by CO₂ sequestration in marine shale: a molecular view based on realistic kerogen model[J]. Arabian Journal of Geosciences, 2018. DOI : 10.1007/s12517-018-3762-5
- [5] Tianyi Z , Xiangfang L , Zhengfu N , et al. Pore structure and adsorption behavior of shale gas reservoir with influence of maturity: a case study of Lower Silurian Longmaxi formation in China[J]. Arabian Journal of Geosciences, 2018, 11(13):353-. DOI : 10.1007/s12517-018-3673-5
- [6] Hassan Mahani, Steffen Berg, et al. Driving Mechanism of Low Salinity Flooding in Carbonate Rocks. Paper SPE 174300. EUROPEC 2015, 1-4 June, Madrid, Spain
- [7] Hadia N J , Ashraf A , Tweheyo M T , et al. Laboratory investigation on effects of initial wettabilities on performance of low salinity waterflooding[J]. Journal of Petroleum Science and Engineering, 2013, 105:18–25. DOI : 10.1016/j.petrol.2013.03.014
- [8] Mahani H , Keya A L , Berg S , et al. Insights into the Mechanism of Wettability Alteration by Low-Salinity Flooding (LSF) in Carbonates[J]. Energy & Fuels, 2015, 29(3):1352-1367.
- [9] Yang J , Dong Z , Dong M , et al. Wettability Alteration during Low-Salinity Waterflooding and the Relevance of Divalent Ions in This Process[J]. Energy & Fuels, 2015:acs.energyfuels.5b01847. DOI : 10.1021/ef5023847
- [10] Mahani H, Menezes R, Berg S, et al. Insights into the Impact of Temperature on the Wettability Alteration by Low Salinity in Carbonate Rocks[J]. Energy & Fuels, 2017, 31(8):7839–7853. DOI : 10.1021/acs.energyfuels.7b00776

Investigation of gamma-ray shielding properties of waste medical glass at 511 keV

Imad H.SHARQI^{1*}, Kadir GÜNOĞLU², Hakan AKYILDIRIM¹, İskender AKKURT¹,
Taner KAVAS³

1 Suleyman Demirel University, Science Faculty, Physics Department, Isparta-TURKEY

2 Isparta University of Applied Sciences, Technical Vocational School, Isparta- TURKEY

3 Afyon Kocatepe University, Department of Materials Science and Engineering, Afyonkarahisar, TURKEY

ABSTRACT

The use of radiation in so many areas has increased the importance of radiation protection. The three basic principles of radiation protection are time, distance and shield. Shield, which is one of these three principles, is a general of different types of materials placed between a human or a system and radiation. Researchers examine the radiation shielding properties of the composite materials they produce by combining different materials.

In this study, the gamma ray shielding properties of the waste medical glass were experimentally measured for 511 keV gamma energy. Measurements were made using a low level gamma counting spectrometer that includes a NaI (TI) detector connected to a multi-channel pulse height analyzer.

KEYWORDS: waste medical glass, gamma ray shielding, NaI (TI) detector

1. INTRODUCTION

Radiation is defined as energy emitted by an unstable atom that travels at the speed of light through space [1]. Radiation is the term for released atomic energy or particles [2]. Nuclear radiation is divided into several types, focusing on whether there is a charge or not, where charged particles represent alpha electrons and positrons [3]. Uncharged particles include photons and protons. Photons consist of gamma rays in a spectrum, beginning with microwaves and ending with gamma rays. The main goal of radiation protection is to prevent or limit radiation exposure. Exposure to ionizing radiation can be achieved in one of two ways: by direct exposure to radiation from a source or through indirect exposure to radiation from a source. As a result, there are three mechanisms to radiation protection [4]. In the event of exposure to an external radiation source or during the period of making the elements radioactive in internal radiation exposure, exposure time is critical [5]. Exposure increases with time and expires with decrease in time. In addition, radiation protection is aided by distance, because the greater the distance from the source of radiation, the lower the amount of radiation exposure [6]. As a result of this ability, materials on radiation attenuation and absorption, numerous materials may be employed to attenuate rays and act as radiation shields. Radiation shields are used to contain radioactive sources and serve as barriers [7]. Where shields depend on the type of radiation and radiation energy [8]. The glass, used in this process, has excellent physical properties such as transparency and hardness, with the commercial property of a small financial cost. These properties have been used as a shield against radiation. Shielding is one of the main methods of radiation protection. Lead was also used to attenuate gamma rays, and the reason for choosing lead is because of its large atomic number [9].

In this study, the gamma ray shielding properties of the waste medical glass were experimentally measured for 511 keV gamma energy. Measurements were made using a low level gamma counting spectrometer that includes a NaI (TI) detector connected to a multi-channel pulse height analyzer.

2. EXPERIMENTAL DETAL

The gamma ray attenuation coefficients of waste medical glass samples produced by adding %20 zinc oxide (ZnO) were measured to present their radiation shielding performance using a gamma spectroscopy system. The block diagram of the gamma spectroscopy system used in the study and the schematic geometry of all the electronic parts (Multi Channel Analyzer (MCA), Amplifier, High

Voltage (HV)) are shown in Figure 1. The radioactive source and detector were sealed with a perforated collimator with a diameter of 5 mm to obtain a linear beam. In addition, the detector is surrounded by a 20 mm thick lead sheath. The measurement spectra obtained by the analyzer with 16384 channels operating according to digital signal processing techniques were analyzed using MAESTRO-32 software [10-12].

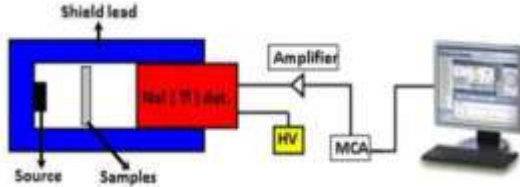


Figure 1. Block diagram and experimental geometry

First, the intensity of the measurement without sample between the source and detector was defined as I_0 . Then, the measurement density made by taking a sample of x thickness between the source and the detector was defined as I . By using these densities obtained as a result of the measurements, linear attenuation coefficient values were calculated using the exponential attenuation law.

$$I = I_0 e^{-\mu x}$$

The number of counts recorded in the detector as an energy spectrum is shown in Figure 2 for 511 keV gamma energy. The difference between the amount of gamma rays collected with and without the glass can be clearly seen .

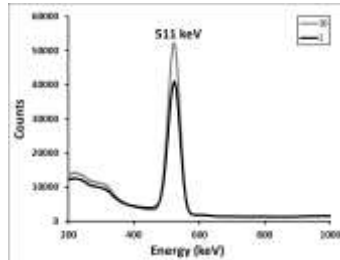


Figure 2. Gamma rays spectrum count with and without the glass.

3. RESULTS AND DISCUSSION

The gamma ray attenuation coefficient for waste medical glass and produced by adding %20 zinc oxide (ZnO) in glass were measured using a gamma spectrometer for 511 keV gamma energy. The results obtained are shown in Figure 3.

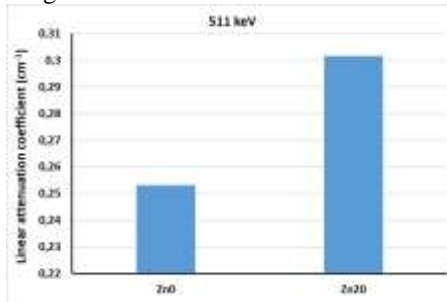


Figure 3. Results of gamma ray attenuation coefficient for glass samples

As seen in Figure 3, adding 20% zinc oxide (ZnO) to waste medical glass increased the gamma ray attenuation coefficient.

REFERENCES

- [1] Akkurt I, Basyigit C, Kilincarslan S, Mavi B (2005) The shielding of γ -rays by concretes produced with barite. *Prog Nucl Energy* 46(1):1–11
- [2] Al-Saadi, A. J., & Saadon, A. K. (2017). Gamma Ray Attenuation Coefficients for Lead Oxide and Iron Oxide Reinforced In Silicate Glasses as Radiation Shielding Windows. *Ibn AL-Haitham Journal For Pure and Applied Science*, 27(3), 201-214.
- [3] Al-Sarray E, Akkurt I, Günoğlu K, Evcin A, Bezir NÇ (2017) Radiation shielding properties of some composite Panel. *Acta Phys Polon A* 132(3):490–492
- [4] Archer, B. R. (2005). Recent history of the shielding of medical x-ray imaging facilities. *Health physics*, 88(6), 579-586.
- [5] Council, F. R. (1960). radiation protection standards. Washington, DC: Govern-ment Printing Office.
- [6] Hofstadter, R. (1949). The detection of gamma-rays with thallium-activated sodium iodide crystals. *Physical Review*, 75(5), 796.
- [7] Kim, J. H. (2018). Three principles for radiation safety: time, distance, and shielding. *The Korean journal of pain*, 31(3), 145.
- [8] Mann, R. B., & Morris, M. S. (1993). Classical models of subatomic particles. *Physics Letters A*, 181(6), 443-445.
- [9] McCaffrey, J. P., Shen, H., Downton, B., & Mainegra-Hing, E. (2007). Radiation attenuation by lead and nonlead materials used in radiation shielding garments. *Medical physics*, 34(2), 530-537.
- [10] I. Akkurt, S.S. Arda, K. Gunoglu Variation of Energy Resolution with Distance for a NaI(Tl) Detector. *Acta Physica Polonica A* 128 -2(2015)422
- [11] I. Akkurt et al. Monte Carlo simulation of a NaI(Tl) detector efficiency. *Rad. Phys. Chem.* 176(2020)109081.DOI: 10.1016/j.radphyschem.2020.109081
- [12] I. Akkurt K. Gunoglu, and S. S. Arda. Detection Efficiency of NaI(Tl) Detector in 511–1332 keV Energy Range. *Science and Technology of Nuclear Installations* (2014) Article ID 186798, 5 pages <http://dx.doi.org/10.1155/2014/186798>

Reinforcement of Glulam Beams with Carbon-FRP

Şemsettin KILINÇARSLAN*, Yasemin ŞİMŞEK TÜRKER

Suleyman Demirel University/Department of Civil Engineering, Isparta, Turkey

*semsettinkilincarslan@sdu.edu.tr

ABSTRACT

Sustainability is a concept that has been used for a long time in the management of forest resources. This concept, which is considered as managing the resources used without losing their qualities, was inspired by the forestry sector and adapted to other sectors. Wood is an organic building material that buildings need a lot and whose raw material source is forests. It is not possible to use no wooden materials (roof, concrete formwork, coating, stairs, furniture, doors, windows, etc.) even in a structure where the entire carrier system is concrete or steel. Waste material generated during the production of wooden structures is very low and can be used in different applications. In addition to being an environmentally friendly material that causes low energy consumption and low air and water pollution in its production, wood continues to maintain the same feature after its useful life. Glued laminated timber (glulam) optimizes the structural characteristics of wood, being itself a versatile material with many possibilities. In this study, the reinforcement of glulam wood composite, which is widely used in the construction of wooden structures, with carbon-based FRP polymer was investigated. 90x90x1300 mm glulam beams are reinforced with carbon-based fiber reinforced polymer composite. It was determined that the load carrying capacities, displacement amounts and flexural strength values of glulam beams increased with the effect of reinforcement with fiber reinforced polymer composites.

KEYWORDS – *Wood materials, Glulam, Reinforced, Flexural properties*

1. INTRODUCTION

Metals and alloys, polymers, ceramics, and composites are the four primary categories of engineering materials [1,2]. The definition of composite material is basically used to specify new types of materials that are formed by the use of two or more materials together and have different properties from the materials from which they are formed [3,4].

Advanced Composites Material ACM, also known as Fiber Reinforced Polymer (FRP), was created as a consequence of research for a new durable material [5,6]. Advanced Composite Technology from the aerospace and other commercial sectors is an engineer's dream in terms of innovative structural design and implementation [7]. In recent years, fiber reinforced polymers have gained importance in various fields as high-performance materials due to their unique properties. These features are excellent mechanical strength, high corrosion resistance, dimensional stability, low assembly cost and light weight. Polymer composite materials are used in aviation, automotive, marine, infrastructure, military industry, aircraft industry, sports equipment and other industries [8]. The material known today as glulam was first used in 1893 in the construction of an auditorium in Basel, Switzerland. Glulam is a building element produced by joining solid timbers side by side and on top of each other to create large dimensions. Pieces are usually created with finger joints. Glulam is superior to solid wood in that it can be produced longer, thicker and wider [9]. Recently, increasing costs and decreasing stocks of high quality lamination have brought the issue of strengthening glulam with FRP more on the agenda. The role of FRP with high mechanical properties is to limit the rupture of defective parts in glulam and prevent cracks from opening [10,11]. Even a thin strip of FRP can increase the flexural strength of glulam by over 100% [12]. In this study, the 3-layer glulam beam element produced from spruce wood was reinforced with carbon fiber reinforced polymer material and the flexural properties of the beams were investigated.

2. MATERIAL AND METHODS

In this study, 3-layer 90 mm x 90 mm x 1300 mm glulam beams produced from spruce wood type timbers were used. The beams used in the study were obtained from Nasreddin Forest Products (Naswood) in Antalya Organized Industry. The dimensions of the supplied glulam beams are given schematically in Figure 1.

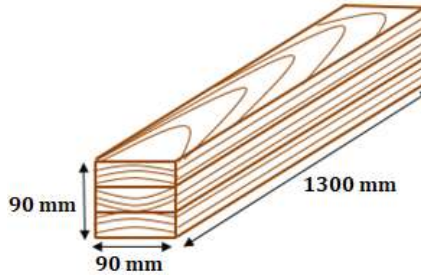


Figure 1. Size of glulam beams subjected to flexural test

Glulam beam is reinforced with carbon-based polymer fabric along the beam. As seen in Figure 2, flexural test was performed on the reinforced beam (CFRP-Glulam) and the reference (R-Glulam) beam in the Construction Laboratory of the Civil Engineering Department of Süleyman Demirel University.



Figure 2. Device for flexural tests of beams

The load-displacement curves of the beams subjected to the flexural test were examined.

3. RESULTS

In the study, flexural properties of glulam beams and reference beams reinforced with FRP polymer were determined. The load-displacement graphs of the beams are given in Figure 3.

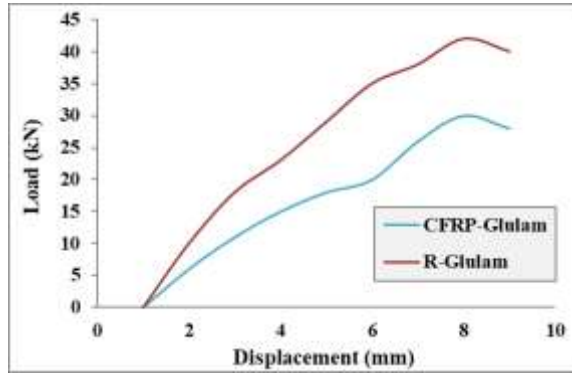


Figure 3. Load-displacement graphic of CFRP-Glulam and R-Glulam beams

As seen in Figure 4, the load carrying capacity of glulam beams reinforced with carbon fiber reinforced polymer fabric increased significantly compared to the reference beams. The load carrying capacity of the reinforced beams increased by 42.85% and the displacement amount increased by 86.61% compared to the reference beams.

4. CONCLUSION

In this study, glulam beams, which are widely used in the wood construction industry, were reinforced with FRP, which has been emphasized in recent years, and the flexural properties of the beams were investigated. The findings showed that the load-bearing capacity and displacement of beams reinforced with fiber-reinforced polymer fabric increased significantly.

The majority of wooden structures nowadays need to be restored and strengthened in a safe manner. Traditional methods of strengthening take time and require ongoing upkeep. Strengthening timber structures with FRP, on the other hand, takes no time and has a pleasing appearance. As a result, the carbon-based FRP polymer fabrics employed in the study are recommended for use in existing and historical wooden structures to strengthen wooden elements.

ACKNOWLEDGEMENTS

This study has been prepared within the scope of the thematic area of "Sustainable Building Materials and Technologies" with SDÜ BAP project with FDK-2019-6950 project code and YÖK 100/2000 doctoral program. The authors thank the SDU BAP unit, YÖK and YÖK100/2000 program staff.

REFERENCES

- [1] S. Karakaya, Tabakalı Kompozit Plakların Gelismis Global Optimizasyon Teknikleriyle Yapısal Optimizasyonu, Yüksek Lisans, Afyonkarahisar Kocatepe Üniversitesi, Fen Bilimleri Enstitüsü, (2007), Afyon.
- [2] Y. Swolfs, I. Verpoest, L. Gorbatikh, Recent advances in fibre-hybrid composites: materials selection, opportunities and applications. *International Materials Reviews*, 64(4), (2019), 181-215.
- [3] M. Y. Solmaz, M. Gür, Tabakalı Kompozit Plakalarda Takviye Malzemesi ve Oryantasyon Açısının Gerilme Analizine Etkisi, *Doğu Anadolu Bölgesi Araştırmaları*, 6 (1), (2007), 16-25.
- [4] L. Van Den Einde, L. Zhao, F. Seible, Use of FRP composites in civil structural applications. *Construction and building materials*, 17(6-7), (2003), 389-403.
- [5] J. R. Correia, Pultrusion of advanced fibre-reinforced polymer (FRP) composites. In *Advanced Fibre-Reinforced Polymer (FRP) Composites for Structural Applications*, (2013), 207-251.

-
- [6] A. R. Mohd Sam, M. Y. Ihsak, S. Abu Hassan, Advanced Composites in Malaysian Construction Industry, Proceedings of the 6th Asia-Pacific Structural Engineering and Construction Conference, 5 – 6 September, Kuala Lumpur, Malaysia, Faculty of Civil Engineering, Universiti Teknologi Malaysia, 152- 158 (2006).
- [7] M. Benjamin, P.E. Tang, FRP Composites Technology Brings Advantages to The American Bridge Bulding Industry, Proceedings published in the 2nd International Workshop on Structural Composites for Infrastructure Applications, December 16-18, (2003), Cairo, Egypt, Office of Bridge Technology.
- [8] A. S. Singha, V. K. Thakur, Physical, Chemical and Mechanical Properties of Hibiscus sabdariffa Fiber/Polymer Composite, International Journal of Polymeric Materials, 58 (4), (2009), 217–228.
- [9] M. Richie, Fatigue Behavior of FRP-Reinforced Douglas- Fir Glued Laminated Bridge Girders, Master, Maine University, Civil Engineering, (2003), Orono.
- [10] V. G. Davids, Nonlinear Analysis of FRP-Glulam-Concrete Bemas with Partial Composite, Journal of Structural Engineering, 127(8), (2001), 967-971.
- [11] A. André, Reserach Report, Fibres for Strengthening of Timber Structures, Luleå University of Technology, Department of Civil and Environmental Engineering, Division of Structural Engineering, ISSN: 1402-1528, (2006), Luleå, Sweden.
- [12] N. Stevens, G. Criner, Department of Resource Economics and Policy University of Maine, Economic Analysis of Fiber-Reinforced Polymer Wood Beams, Bulletin, ISSN 1070–1494. June 2000.

The 40K natural radionuclide concentration in some medicinal aromatic plants

Sıme ÇABUK1*, Erman DUMAN1, Kadir GÜNOĞLU2, İskender AKKURT3

1University of Afyon Kocatepe, Department of Food Engineering, Faculty of Engineering, Afyonkarahisar, TURKEY

2 Isparta University of Applied Sciences, Technical Sciences Vocational School, Isparta-TURKEY,

3 Suleyman Demirel University, Physics Department, Isparta, TURKEY,

ABSTRACT

In addition to singly occurring radionuclides such as 40K, natural radioactive decay such as the 238U and 232Th series is found at various levels in the atmosphere and on the earth. Radioactivity in farmland and soil can pass to surrounding plants. The radionuclide in the environment is transferred to the plants indirectly from the soil through the roots. When food plants thrive in a polluted soil, the activity moves from the soil to the roots and then to the stem or leaves of the plant. It eventually makes its way into the human diet. This radionuclide can enter plants during mineral uptake with nutrients and accumulate in different areas and even reach edible parts. The aim of this study is to measure the 40K activity concentration in some aromatic plants used by humans both as tea and as a spice. The measurement was performed using a NaI(Tl) detector at spectrometry laboratory of Süleyman Demirel University. The results of the activity concentrations obtained from the measurements were compared with the mean values.

Keywords: 40K natural radionuclide, medicinal aromatic plants, NaI(Tl) detector

1. INTRODUCTION

Natural radionuclide concentrations in environmental samples vary depending on geographical and geological factors [1]. Natural sources of radioactivity in the environment are divided into two groups as terrestrial and cosmic origin and are called NORM (natural radioactive substances in nature) [2]. Humans are exposed to radiation dose both internally and externally from these natural sources. Internal exposures result from the ingestion of terrestrial radionuclides by inhalation and ingestion. The inhalation exposure is due to the presence of airborne dust particles containing radionuclides of the 238U and 232Th decay series. The greatest contribution to inhalation exposure comes from the short half-life of radon degradation products. Ingestion exposure is mostly due to 238U and 232Th series radionuclides and 40K in food and drinking water.

Medicinal plants have been used by humans for centuries in the treatment of diseases within cultures and on all continents. Recently, medicinal plant studies have enabled comprehensive studies to be carried out all over the world due to the diversity of medicinal plants and their wide potential in drug production. Generally, studies of medicinal plants aim to characterize the active components of plants. However, studies on the determination of natural radioactivity levels in such plants are scarce in the literature. As humanity, the use of traditional herbal medicines for the treatment of various diseases makes studies on the determination of radionuclide concentrations in such plants very important [3,4].

In the literature, there are studies conducted in various countries on the determination of radioactivity levels in plant samples such as medicinal plants [3], chamomile [5], tea [5,6], emerald wave flower [4], hazelnut [7], pine needle [8]. In this study, Potassium-40 activity concentrations of some medicinal aromatic plants were measured by using NaI (Tl) detector gamma spectroscopy system.

2. MATERIAL AND METHOD

In this study, medicinal aromatic plants (Rosemary, Daisy, Green Tea, Lavender, Bay) were ground and dried until 1000C in an oven for about 24 h. The dried samples have been filled in a cup which

is sealed tightly with a thick tape around its neck to limit any gas escape from it, and stored for four weeks to get secular equilibrium to be achieved between ²³⁸U and its progeny [9]. The radioactivity concentration of ⁴⁰K in medicinal aromatic plants were determined using a gamma ray spectrometry consists of a 3”x3” NaI(Tl) detector connected to Multi-Channel-Analyser (MCA). The spectrum is analyzed using the MAESTRO32 obtained from ORTEC. The schematic view of the experimental system has been shown in Figure 1.

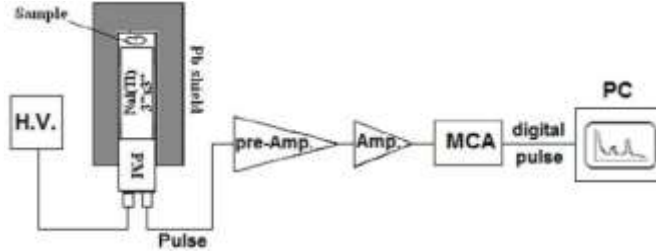


Figure 1. Schematic view of gamma Spectrometer and electronic units

Before measurement the system should be calibrated. This is done using ¹³⁷Cs and ⁶⁰Co radioactive sources, which produce γ -ray energy of 662, 1173 and 1332 keV, respectively. The γ -ray spectrum obtained from the mentioned source and related fit has been displayed in Figure 2 (a). Detection efficiency calibration was done based on two variables. The first of these variables is the distance between the detector and the radioactive source. This distance was taken as 0.5 cm. The second variable is different gamma ray energies. Six different gamma ray energies were used when determining the detection efficiency calibration. The detection efficiency calibration values obtained depending on these variables are shown in Figure 2 (b) [12]. As can be seen from Figure 3, the efficiency values are consistent since the R2 value is close to 1.

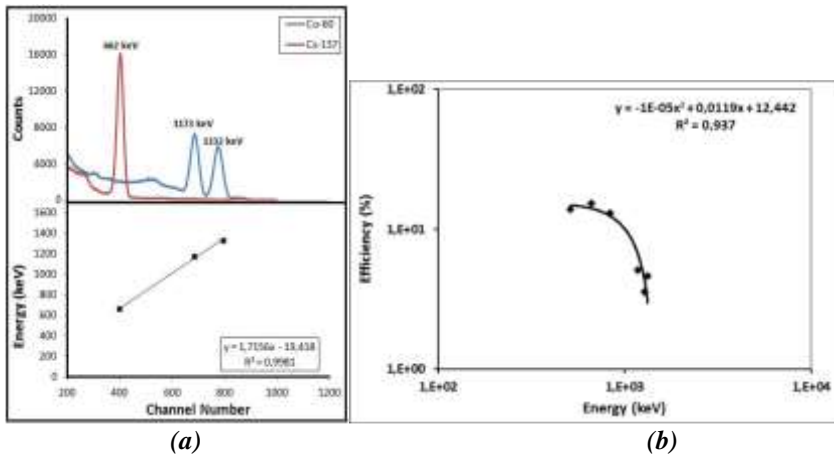


Figure 2. (a) The γ -ray energy spectrum obtained from ¹³⁷Cs and ⁶⁰Co sources (upper) and related fit channel versus energy (keV). (b) Detection efficiency depending on gamma ray energies

The activities for the natural radionuclides were calculated using the following relation [4]

$$A (Bq/kg) = \frac{N}{E_{\gamma} \cdot P_{\gamma} \cdot t \cdot M_S}$$

where A is the activity of the radionuclide in Bq/kg, N is the net peak area under the most prominent photo peaks calculated by subtracting the respective count rate from the background spectrum obtained for the same counting time. The net count rate in the measurement is calculated from the background subtracted area of prominent gamma ray peaks. E_{γ} is the detector efficiency of the specific gamma ray, P_{γ} the absolute transition probability of gamma decay, t the counting time (s) and Ms the mass of the sample (kg).

3. RESULTS AND DISCUSSION

The activity concentration of ^{40}K obtained from measurements using gamma spectroscopy is shown in Figure 3. These results showed that the activity concentration of ^{40}K ranged from 43,881 to 250,101 Bq / kg. The mean value of the ^{40}K activity concentration was measured as 185,898 Bq / kg.

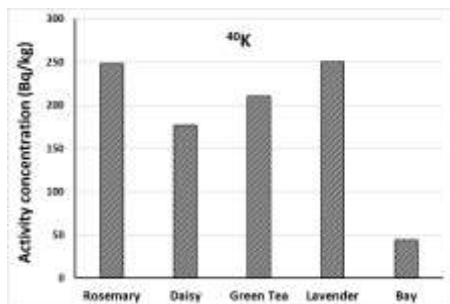


Figure 2. The activity concentration of ^{40}K in gravel samples

REFERENCES

- [1] Badran, H.M., Sharshar, T., Elnimer, T., 2003. Levels of ^{137}Cs and ^{40}K in edible parts of some vegetables consumed in Egypt. *J Radioanal Nucl Chem* 67:181-190.
- [2] Kathren, R.L., 1998. NORM Sources and Their Origins. *Appl Radiat Isot* 49(3):149-168.
- [3] Desideri, D., Meli, M.A., Roselli, C., 2010. Natural and artificial radioactivity determination of some medicinal plants. *Journal of Environmental Radioactivity* 101:751-756.
- [4] Sussa, F.V., Damatto, S.R., Alencar, M.M., Mazzilli, B.P., Silva, Paulo S.C., 2013. Natural radioactivity determination in samples of *Peperomia pellucida* commonly used as a medicinal herb. *Journal of Environmental Radioactivity* 116:148-151.
- [5] Desideri, D., Meli, M.A., Roselli, C., Feduzi, L., 2011. Alpha and gamma spectrometry for determination of natural and artificial radionuclides in tea, herbal tea and camomile marketed in Italy. *Microchemical Journal* 98: 170-175.
- [6] Görür, F.K., Keser, R., Akçay, N., Dizman, S., Okumuşoğlu, N.T., 2011. Radionuclides and heavy metals concentrations in Turkish market tea. *Food Control* 22: 2065-2070.
- [7] Cevik, U., Celik, N., Celik, A., Damla, N., Coskuncelebi, K., 2009. Radioactivity and heavy metal levels in hazelnut growing in the Eastern Black Sea Region of Turkey. *Food and Chemical Toxicology* 47: 2351-2355.
- [8] Karadeniz, Ö., Yaprak, G., 2007. Distribution of radiocesium and natural gamma emitters in pine needles in coniferous forest sites of Izmir. *Applied Radiation and Isotopes* 65: 1363-1367.
- [9]. Akkurt, I., Oruncak, B., Gunoglu, K., 2010. Natural radioactivity and dose rates in commercially used marble from Afyonkarahisar – Turkey. *International Journal of the Physical Sciences* Vol. 5 (2), p:170-173.
- [10]. I.Akkurt, K. Gunoglu, S.S. Arda, Detection Efficiency of NaI(Tl) Detector in 511–1332 keV Energy Range. *Sci. Technol.Nucl. Install.* 2014, 186798 (2014).

Investigation of Radiation Shielding Properties of Wood Material

Şemsettin KILINÇARSLAN^{1*}, İskender AKKURT², Yasemin ŞİMŞEK TÜRKER¹, Kadir GÜNOĞLU³

¹Suleyman Demirel University, Civil Engineering Department, Isparta-TURKEY

²Suleyman Demirel University, Physics Department, Isparta, TURKEY

³Isparta University of Applied Sciences, Technical Sciences Vocational School, Isparta-TURKEY

*semsettinkilincarslan@sdu.edu.tr

ABSTRACT

Radiation is a phenomenon that always exists in nature and we live together. With the development of technology, radiation has started to be used frequently in fields such as medicine, energy and industry, and therefore studies on radiation are increasing. Radiation protection methods have gained importance, especially since radiation is harmful to living things. These methods are distance, time and shielding. Shielding, the most important of these methods, is based on placing an obstacle between the system to be protected from radiation and the radiation source. For this reason, the researchers produced different materials for shielding radiation and examined the radiation absorption properties of these materials. Wood material is preferred because it is a renewable resource, the amount of energy used in the production of wooden building elements and structures is low, and the amount of carbon dioxide produced in the production process is close to zero. It is seen that the wooden material, which we have seen in the past especially in housing construction, is widely used in the production of multi-storey buildings with new production technologies. Studies have been carried out on the radiation shielding properties of wood building materials, which are frequently used in building construction in recent years. In this study, radiation shielding properties of radial and tangential sawn timbers obtained from Red Pine tree (*Pinus brutia* Ten.) species were investigated. It was determined that the radiation shielding properties of radial and tangential sawn timbers gave similar results.

KEYWORDS – Wood materials, Radiation Shielding, tangential, radial

1. INTRODUCTION

Radiation exposure consists of two separate components, internal (natural) and external exposure. Natural radiation varies widely between fields. However, when the radiation source is concentrated and confined to a particular area, human exposure to radiation from that source can be reduced through the use of carefully designed systems and procedures [1, 2].

Recently, a lot of research has been done on the radiation protection properties of different materials using theoretical methods. Some examples are summarized as follows; The mass attenuation coefficient (MAC) of boric acid was examined by İçelli et al., (2004) [3] at various concentrations. Jalali and Mohammadi (2008) [4] measured boric acid attenuation coefficients in the energy range of 662 to 1408 keV. Agar et al. (2019) [5] looked at the linear attenuation coefficient (LAC), mass attenuation coefficient (MAC), and half value layer (HVL) of perlite added concretes in the energy range of 81 to 1333 keV. In an energy range of 13.94 to 88.04 keV, Akman et al. (2019) [6] determined the MAC and radiation protection efficiency of various soils. At a photon energy of 662 keV, Salama and Maher (2019) [7] investigated the mass attenuation coefficient of glass materials. At a photon energy of 662 keV, Salama and Maher (2019) [8] investigated the mass attenuation coefficient of glass materials. A study on the MAC of various building materials including as asbestos, clay brick, brick, and wood was conducted by Salinas et al., (2006) [9]. At a photon energy of 59.54 keV, Bradley et al. (1991) [10] studied the gamma-ray linear attenuation coefficient of various tropical wood densities ranging from 135 to 1180 kg/m³. With increasing wood densities, the LAC values have risen. The LAC of wood from *Rhizophora* spp. (1040 kg/m³) was determined

to be 0.212 cm/1. When compared to water, the LAC value of *Rhizophora* spp. wood was 0.205 cm/1.

One of the factors that has the most important effect on the quality of wood material is the direction of mowing. In tangential sawn timber, the cutting direction is tangent to the annual rings of the log at a certain distance from the core. In radial sawn timber, the mowing direction is perpendicular to the annual rings. The properties of the wood material change according to the cutting direction of the log. In this study, radiation shielding properties of radial and tangential sawn red pine (*Pinus brutia* Ten.) timbers were investigated.

2. MATERIAL AND METHODS

In this study, red pine (*Pinus brutia* Ten.) timbers obtained from the forest products company in Isparta province were used as wood material. It has been ensured that this timber provided is perfect and that the fibers are smooth, without backing, without reaction wood, and has not suffered from fungal and insect damages. Samples of 2 (thickness) x10 (width) 10 (length) cm were cut from tangential and radial sawn timbers with a motorized chainsaw. The schematic images of the samples whose radiation shielding coefficient are to be determined are given in Fig. 1.

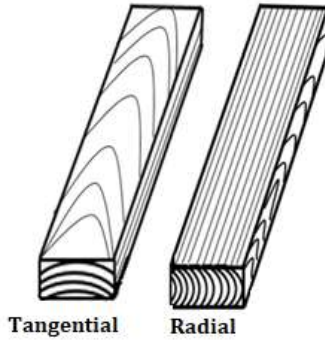


Fig. 1. Image of radial and tangential cut test specimens

Radial and tangential sawn timbers obtained were determined by radiation shielding values. The linear attenuation coefficients of tangential and radial sawn red pine timber were measured using gamma spectrometer containing NaI(Tl) detector. The radiation source was emitting 662 keV, 1173 keV and 1332 keV gamma rays.

From the spectrum obtained from detector the linear attenuation coefficients are determined using the Beer–Lambert formula

$$I = I_0 e^{-\mu x} \quad (1)$$

Here μ is the linear attenuation coefficient, (x) thickness, (I_0) number of gamma quanta emitted from source and (I) is number of gamma quanta hitting detector.

3. RESULTS

The radiation shielding properties of Pine wood are given in Fig. 2.

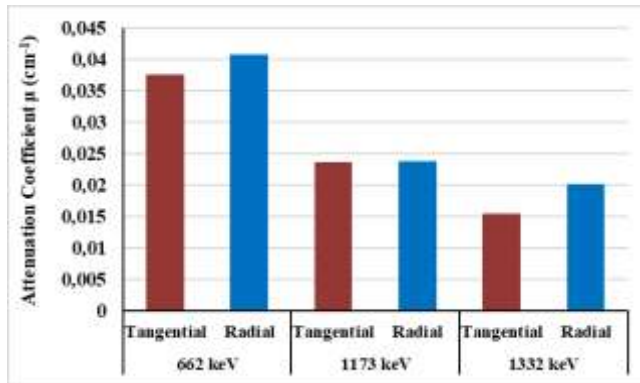


Fig. 2. Radiation shielding properties of Pine wood

When Figure 2 is examined, it has been determined that the linear damping coefficient values in the radial direction are higher than the values in the tangential direction. It was determined that the radiation shielding values determined in the radial direction increased by 8.43% in the 662 keV energy range, 0.51% in the 1173 keV energy range and 30.75% in the 1332 keV energy range, according to the tangential direction.

4. CONCLUSION

In our world where resources are getting scarce, insulation technologies are of great importance. Materials produced using insulation materials are both economical and healthy. In this study, the radiation shielding property of untreated wood material was investigated depending on the directions. In this study, it was determined that radial sawn timbers with very little effect had higher radiation retention. For this reason, while creating the design of the structures, structural designs should be carried out considering the high radiation retention feature of radial sawn timbers.

ACKNOWLEDGEMENTS

This study has been prepared within the scope of the thematic area of "Sustainable Building Materials and Technologies" with SDÜ BAP project with FDK-2019-6950 project code and YÖK 100/2000 doctoral program. The authors thank the SDU BAP unit, YÖK and YÖK100/2000 program staff.

REFERENCES

- [1] M. Erdem, O. Baykara, M. Dođru, F. Kuluöztürk, A novel shielding material prepared from solid waste containing lead for gamma ray. *Radiation Physics and Chemistry*, 79(9), (2010), 917-922. <https://doi.org/10.1016/j.radphyschem.2010.04.009>
- [2] I. Akkurt, R. B. Malidarre, T. Kavas, Monte Carlo simulation of radiation shielding properties of the glass system containing Bi₂O₃. *The European Physical Journal Plus*, 136(3), (2021), 1-10.
- [3] O. İçelli, S. Erzeneođlu, R. Boncukçuođlu. Experimental studies on measurements of mass attenuation coefficients of boric acid at different concentration. *Annals of Nuclear Energy*, 31(1), (2004), 97-106. [https://doi.org/10.1016/S0306-4549\(03\)00171-3](https://doi.org/10.1016/S0306-4549(03)00171-3)
- [4] M. Jalali, A. Mohammadi, Gamma ray attenuation coefficient measurement for neutron-absorbent materials. *Radiation Physics and Chemistry*, 77(5), (2008), 523-527. <https://doi.org/10.1016/j.radphyschem.2007.12.014>
- [5] O. Agar, H. O. Tekin, M. I. Sayyed, M. E. Korkmaz, O. Culfa, C. Ertugay, Experimental investigation of photon attenuation behaviors for concretes including natural perlite mineral.

-
- Results in Physics, 12 (November 2018), (2019), 237-243. <https://doi.org/10.1016/j.rinp.2018.11.053>
- [6] F. Akman, V. Turan, M. I. Sayyed, F. Akdemir, M. R. Kaçal, R. Durak, M. H. M. Zaid, Comprehensive study on evaluation of shielding parameters of selected soils by gamma and X-rays transmission in the range 13.94-88.04 keV using WinXCom and FFAST programs. Results in Physics, 15 (August), (2019), 102751. <https://doi.org/10.1016/j.rinp.2019.102751>
- [7] E. Salama, A. Maher, Application of GATE/GEANT 4 code in investigation of gamma shielding effectiveness of glass materials. Journal of Physics: Conference Series, 1253(1), (2019). <https://doi.org/10.1088/1742-6596/1253/1/012032>
- [8] B. Aygün, High alloyed new stainless steel shielding material for gamma and fast neutron radiation. Nuclear Engineering and Technology, 52(3), (2020), 647-653. <https://doi.org/10.1016/j.net.2019.08.017>
- [9] I. C. P. Salinas, C. C. Conti, R. T. Lopes, Effective density and mass attenuation coefficient for building material in Brazil. Applied Radiation and Isotopes, 64(1), (2006), 13-18. <https://doi.org/10.1016/j.apradiso.2005.07.003>
- [10] D. A. Bradley, A. A. Tajuddin, C. W. A. C. W. Sudin, S. Bauk, Photon attenuation studies on tropical hardwoods. International Journal of Radiation Applications and Instrumentation. Part, 42(8), (1991), 771-773. [https://doi.org/10.1016/0883-2889\(91\)90182-Z](https://doi.org/10.1016/0883-2889(91)90182-Z)

Experimental investigation of biomaterials for gamma ray protection

Aycan SAHİN^{1*}, Kadir GÜNOĞLU², Hakan AKYILDIRIM³, İskender AKKURT³

¹Akdeniz University, Vocational School of Health Services, Antalya-TURKEY

²Department of Physics, Suleyman Demirel University, Isparta- TURKEY,

³Isparta University of Applied Sciences, Technical Sciences Vocational School, Isparta-TURKEY

ABSTRACT

In this paper, the linear attenuation coefficient of biomaterials was measured for gamma rays of energy 662 keV. The gamma rays for these of energy have been obtained from ¹³⁷Cs point source. The measurement has been performed using a well calibrated gamma ray spectrometer which consists of 3“x3” NaI(Tl) scintillation detector, Amplifier and Computerized gamma spectrum analysis carts

KEYWORDS: Linear attenuation, biomaterials, NaI(Tl) scintillation detector

1. INTRODUCTION

The implantation of orthopedic biomaterials is widely used all around the globe to restore physiological functions. Approximately 70% of the implants used in medicine are metallic biomaterials and are mainly used to repair failed hard tissue. The demand for implants is increasing exponentially as part of the efforts to improve the life quality of the aging population [1]. The three most implanted metallic biomaterials are titanium alloys (TA), cobalt- chromium alloys (CCA) and stainless steel (SS).

The 316 L SS is the most widely used alloy mainly for non-permanent implants (e.g. bone plates, screws) and dental surgery [2,3]. Despite 316 L SS having good mechanical properties, good biocompatibility and being inexpensive, this alloy is less used for permanent implantation due to the corrosion induced by the contact with body fluids and the release of toxic ions such as nickel and chromium ions which causes local inflammation [4–6]. Among all the SS implants that failed, more than 90% presented corrosion attack [7].

Though a large number of titanium alloys have been developed, they can be grouped into threemajor categories such as α -alloys, β -alloys and $\alpha+\beta$ alloys. Their properties are dependent on microstructure which, in turn, depends on the chemical composition and thermomechanical processing [8].

Due to their high specific strength and exceptional corrosion resistance, titanium alloys have been widely used in engineering, namely in the aerospace, automotive and biomedical fields [9,10]. The alloy Ti-6Al-4V, due to its biocompatibility coupled with good combination of mechanical and corrosive properties, is the most popular titanium based material in the manufacture of biomedical components, including dental implants, prosthetic femoral components, surgical instruments, etc. [11-13].

Cobalt–chromium based alloys have been widely used in various orthopedic implants as well as for manufacturing of metal framework of fixed dental prosthesis because of their excellent mechanical properties, high corrosion and wear resistance, and good biocompatibility. The chemical composition of dental Co-Cr alloys consists of 53–67% Co, 25–32% Cr, 2–6% Mo and small quantities of W, Si, Al and others [14].

In this paper, the linear attenuation coefficient of biomaterials was measured for gamma rays of energy 662 keV. The gamma rays for these of energy have been obtained from ¹³⁷Cs point source. The measurement has been performed using a well calibrated gamma ray spectrometer which consists of 3“x3” NaI(Tl) scintillation detector.

2. EXPERIMENTAL PROCEDURE

The gamma ray attenuation coefficient of biomaterials have been performed using the gamma spectrometer, containing a 3” × 3” inch sodium iodide with thallium (NaI (Tl)) detector, coupled to a digital spectrum analyzer (DSPEC LF), connected to the 16k channels Multi Channel Analyzer (MCA) provided by ORTEC hardware, controlled by MAESTRO32 software (Figure 1).

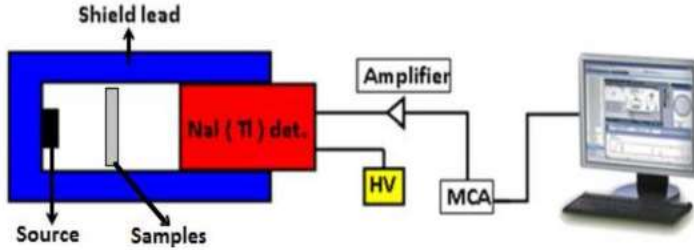


Figure 1. Schematic view of the gamma-ray spectrometer

Detection efficiency calibration was done based on two variables. The first of these variables is the distance between the detector and the radioactive source. This distance was taken as 0.5 cm. The second variable is different gamma ray energies. Six different gamma ray energies were used when determining the detection efficiency calibration. The detection efficiency calibration values obtained depending on these variables are shown in Figure 2 [12]. As can be seen from Figure 3, the efficiency values are consistent since the R2 value is close to 1.

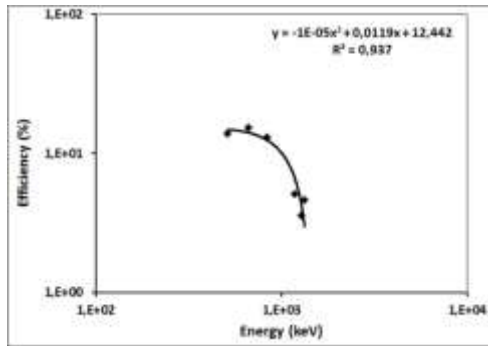


Figure 2. Detection efficiency depending on gamma ray energies

The gamma ray attenuation coefficients μ (cm-1) is obtained by:

$$\mu = \frac{1}{x} \ln \frac{I_0}{I} \tag{1}$$

where x is the material thickness and I and I0 are the background subtracted number of counts recorded in detector with and without material between detector and source, respectively.

3. RESULTS AND DISCUSSION

The linear attenuation coefficient for three different biomaterials was obtained using gamma spectrometry. The results obtained are shown in Figure 3.

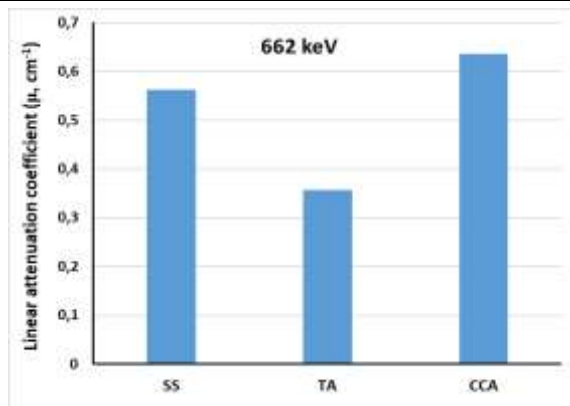


Figure 3. Linear attenuation coefficient results for biomaterials

As seen in Figure 3, among the three different biomaterials, the cobalt-chromium alloy has the highest linear attenuation coefficient and the titanium alloy has the lowest linear attenuation coefficient.

REFERENCES

- [1] M. Niinomi, M. Nakai, J. Hieda, Development of new metallic alloys for biomedical applications, *Acta Biomater.* 8 (11) (2012) 3888–3903.
- [2] A.M. Kumar, S. Nagarajan, S. Ramakrishna, P. Sudhagar, Y.S. Kang, H. Kim, Z.M. Gasem, N. Rajendran, Electrochemical and in vitro bioactivity of polypyrrole/ ceramic nanocomposite coatings on 316L SS bio-implants, *Mater. Sci. Eng. C-Mater. Biol. Appl.* 43 (2014) 76–85.
- [3] Y.C. Su, C. Luo, Z.H. Zhang, H. Hermawan, D.H. Zhu, J.B. Huang, Y.H. Liang, G.Y. Li, L.Q. Ren, Bioinspired surface functionalization of metallic biomaterials, *J. Mech. Behav. Biomed. Mater.* 77 (2018) 90–105.
- [4] M. Navarro, A. Michiardi, O. Castaño, J.A. Planell, Biomaterials in orthopaedics, *J. R. Soc. Interface* 5 (27) (2008) 1137–1158.
- [5] V.K. Balla, M. Das, S. Bose, G.D. Ram, I. Manna, Laser surface modification of 316 L stainless steel with bioactive hydroxyapatite, *Mater. Sci. Eng. C Mater. Biol. Appl.* 33 (8) (2013) 4594–4598.
- [6] S. Sutha, K. Kavitha, G. Karunakaran, V. Rajendran, In-vitro bioactivity, biocorrosion and antibacterial activity of silicon integrated hydroxyapatite/chitosan composite coating on 316 L stainless steel implants, *Mater. Sci. Eng. C Mater. Biol. Appl.* 33 (7) (2013) 4046–4054.
- [7] A. Bekmurzayeva, W.J. Duncanson, H.S. Azevedo, D. Kanayeva, Surface modification of stainless steel for biomedical applications: revisiting a century-old material, *Mater. Sci. Eng. C-Mater. Biol. Appl.* 93 (2018) 1073–1089.
- [8] Y. Luo, In: *Biotribology*, ed. by J.P. Davim (ISTE-Wiley, London, 2010), p. 157.
- [9] M. Ribeiro, M. Moreira and J. Ferreira, Optimization of titanium alloy (6Al–4V) machining, *Journal of Materials Processing Technology* 143 (2003) 458–463.
- [10] M. Rahman, Z. Wang and Y. Wong, A Review on High-Speed Machining of Titanium Alloys, *JSME International Journal Series C Mechanical Systems, Machine Elements and Manufacturing* 49 (2006) 11–20
- [11] V. Latysh, G. Krallics, I. Alexandrov and A. Fodor, Application of bulk nanostructured materials in medicine, *Current Applied Physics* 6 (2006) 262–266.
- [12] R. B. Silva, Performance of different cutting tool materials in finish turning of Ti-6Al-4V alloy with high pressure coolant supply technology (Faculdade de Engenharia Mecanica Universidade Federal de Uberlandia, 2006)

- [13] P. Arrazola, A. Garay, L.M. Iriarte, M. Armendia, S. Marya and F. Le Maitre, Machinability of titanium alloys (Ti6Al4V and Ti555.3), Journal of Materials Processing Technology 209 (2009) 2223-2230.
- [14] Podrrez-Radziszewska M., Haimann K., Dudzinski W., Morawska-Soltysik M., Characteristic of intermetallic phases in cast dental CoCrMo alloy. Archives of Foundry Engineering, 10/3 (2010), 51 – 59.
- [15]. I.Akkurt, K. Gunoglu, S.S. Arda, Detection Efficiency of NaI(Tl) Detector in 511–1332 keV Energy Range Sci. Technol.Nucl. Install. 2014, 186798 (2014).